Nano Today 30 (2020) 100825

Contents lists available at ScienceDirect

Nano Today

journal homepage: www.elsevier.com/locate/nanotoday

Review

Nanofabrication approaches for functional three-dimensional architectures

Hangbo Zhao[a,1], Yongjun Lee[b,1], Mengdi Han[a,1], Bhupendra K. Sharma[b], Xuexian Chen[a,c], Jong-Hyun Ahn[b,*], John A. Rogers[a,d,*]

[a] Center for Bio-Integrated Electronics, Northwestern University, Evanston, Illinois, 60208, USA
[b] School of Electrical and Electronic Engineering, Yonsei University, 50 Yonsei-ro, Seoul 03722, Republic of Korea
[c] Academy for Advanced Interdisciplinary Studies, Peking University, Beijing, 100871, China
[d] Departments of Materials Science and Engineering, Biomedical Engineering, Chemistry, Mechanical Engineering, Electrical Engineering and Computer Science, Simpson Querrey Institute for Nano/Biotechnology, Northwestern University, Evanston, Illinois, 60208, USA

ARTICLE INFO

Article history:
Received 12 August 2019
Received in revised form
18 September 2019
Accepted 9 December 2019
Available online 20 December 2019

ABSTRACT

Three-dimensional (3D) functional systems with sizes in the micro- and nanometer regime are of growing importance across a wide range of electrical, optical, and biological contexts. The unique functionalities of such platforms follow from engineering the shapes, geometries, and architectures of materials into 3D layouts. The main challenges are in developing techniques/methods with sufficient levels of resolution and with broad materials compatibility. The most successful routes include (1) top-down schemes that involve masking and selective material removal, often in repetitive sequences, (2) bottom-up strategies that rely on component assembly or materials deposition, (3) two-dimensional (2D) to 3D shape transformations triggered by internal forces or external stimuli, and more recently, (4) mechanically guided assembly driven by substrate deformations. This review highlights recent progress in these areas, with a focus on techniques with demonstrated capabilities in constructing functional 3D structures and/or devices with key dimensions in the nanoscopic regime, and on their demonstrated or potential applications.
© 2019 Elsevier Ltd. All rights reserved.

Contents

* Corresponding authors.
E-mail addresses: ahnj@yonsei.ac.kr (J.-H. Ahn), jrogers@northwestern.edu (J.A. Rogers).
[1] These authors contributed equally.

https://doi.org/10.1016/j.nantod.2019.100825
1748-0132/© 2019 Elsevier Ltd. All rights reserved.

Introduction

Three-dimensional (3D) functional structures are of considerable interest due to their potential utility in a broad range of applications, from macroscale devices with unconventional engineering designs (e.g., foldable solar panels and retractable roofs) to more challenging and sophisticated devices that incorporate micro/nanoscale features [1–5] (e.g., light tracking photodetectors [6,7] and functional biosensors [8–12]). In these application examples, the 3D architectures of the structures provide unique and important types of functionality beyond those achievable with planar systems. Examples include optical devices that can sense and interact with electromagnetic waves in 3D space [6,13], energy storage devices with high areal energy density arising from the large surface areas of 3D structures [14,15], and biomedical devices that interface seamlessly with intrinsically 3D biological systems [9,11,12].

Such complex 3D structures, especially those with nanoscale dimensions, are difficult to achieve through extensions of the types of methods used in conventional two-dimensional (2D) microsystems technologies, where fabrication occurs through a sequence of layer-by-layer processing steps based on planar substrates. As a result, different approaches must be developed to achieve 3D forms in relevant materials with specific active or passive function. Selective patterning and material removal from bulk materials and guided assembly of micro/nanoscale entities, sometimes referred to as top-down and bottom-up approaches, respectively, represent the most well studied approaches. A key distinction between top-down and bottom-up approaches, as we define them here, is that the former exploits deterministic schemes that operate based on spatially selective removal of material while the latter relies on guided assembly, directed growth or controlled deposition.

In top-down approaches, the removal of selective regions typically occurs through holographic, phase-mask and multiphoton lithography to pattern the application of dry and wet etching processes. In each case, the lithography approach and/or etching technique match requirements set by the materials types and the geometrical features. In this way, a wide range of materials including silicon [16,17], metals [18,19], and polymers [20–22] can be transformed into sophisticated 3D nanostructures. In bottom-up approaches, guided assembly occurs through selective chemical affinity or functionalization among micro/nanoscale entities to form various 3D shapes such as micelles [23,24], DNA-based trusses [25], and metal helices [26].

As alternatives to these top-down and bottom-up approaches, 3D nanostructures can be realized by assembly and transformation dictated by internal or external forces or by mechanically directed processes mediated by a supporting substrate. The latter typically involve release of residual stresses formed during growth/deposition [27–31], light induced actuation of materials such as trans-cis isomerization of azobenzene moieties [32] or glass transitions of polymers [33], expansion/contraction caused by changes in temperature [34,35], pH [36,37] or exchange of surrounding solvents [38–42]. The results can initiate self-folding/rolling deformations in engineered thin film materials or structures, into desired 3D constructs. For example, internal stress/strain in thin film material stacks can result in guided formation of cylinders, spirals, scrolls and other 3D structures, controlled by the location and magnitude of the developed strain and the release geometry. The level of control and the range of 3D architectures can be expanded when applied to designs inspired by concepts in origami/kirigami [13,43–46] to yield advanced 3D nanostructures for various applications [47–52]. These approaches include the formation of cuts in thin layers through patterning and folding/unfolding through external mechanical stimulation, thereby providing versatile design options for responsive and tunable 3D structures.

More recent research demonstrates collections of techniques that exploit mechanically guided processes where compressive buckling induced by an elastomeric substrate [53–55] geometrically transforms planar structures into complex 3D architectures [56–59]. Such strategies can produce sophisticated 3D systems with precisely engineered electrical [60–62], optical [63,64], and biological [65,66] function in rigid, flexible, and even fully stretchable configurations [67,68]. Additional progress expands the range of constituent materials and device components with feature sizes ranging from nanometers to centimeters, where options include mechanical flexibility at the system level through designs that avoid fracture or degradation in properties and that exploit unusual engineering designs in nanoscale architectures [69,70].

This article reviews recent progress on the most advanced forms of these techniques in the formation of 3D functional structures with nanoscale features or with the clear potential to be scaled to these size regimes. Sections 1 and 2 discuss direct fabrication routes from thin film materials or multilayered stacks in various top-down approaches, and the self-assembly of molecules or other small-scale components as examples of bottom-up approaches. Next, other types of 3D nanostructures formed via mechanical assembly processes triggered by internally or externally derived forces, and those associated with compressive buckling, appear in Section 3 and 4, respectively. The latter section additionally highlights examples of functional device integration, with examples that offer fully reversible stretchability, as both a useful mechanical attribute and a means to tune the properties of devices and systems. The paper concludes with content in Section 5 that summarizes the current status of the field and provides perspectives on trends for future work.

Top-down techniques

Top-down techniques rely on methods such as lithographic patterning and selective material removal to produce features with desired shapes and sizes using schemes built on and adapted from processes that form the foundations for manufacturing in the semiconductor industry. An advantage of these strategies is that they leverage well-established techniques to form 3D objects with engineering control and precise placement, without the need for additional assembly or manipulation steps. This section highlights some of the most recent and advanced examples of 3D structures that incorporate nanoscale features and result from combinations of lithography, etching and/or conformal deposition, to guide the addition or removal of materials in a sequential fashion.

A variety of 3D structures formed in this way can be useful in nanoelectronic circuits [71,72], photonic structures [19,73,74], optoelectronic devices [75], microelectromechanical systems (MEMS) [76], biomedical devices [77–79], and metamaterials [80,81]. Well-developed approaches include but are not limited to electron beam lithography [82], multiphoton lithography [83], nanoimprint lithography [84] and holographic lithography [85], each of which can be combined with etching [16,86,87] and/or conformal deposition [88,89] techniques to expand the range of accessible materials and structure dimensions. Comprehensive reviews on 3D nanostructures based on these approaches appear in other articles [90–98].

Many recent advances in lithography-based top-down techniques focus on incorporating functional materials motivated by relevant applications in energy systems, nanofluidic constructs, biosensors and others. One example is in the fabrication of 3D nanostructured electrodes for batteries through holographic lithography, also known as interference lithography. This type

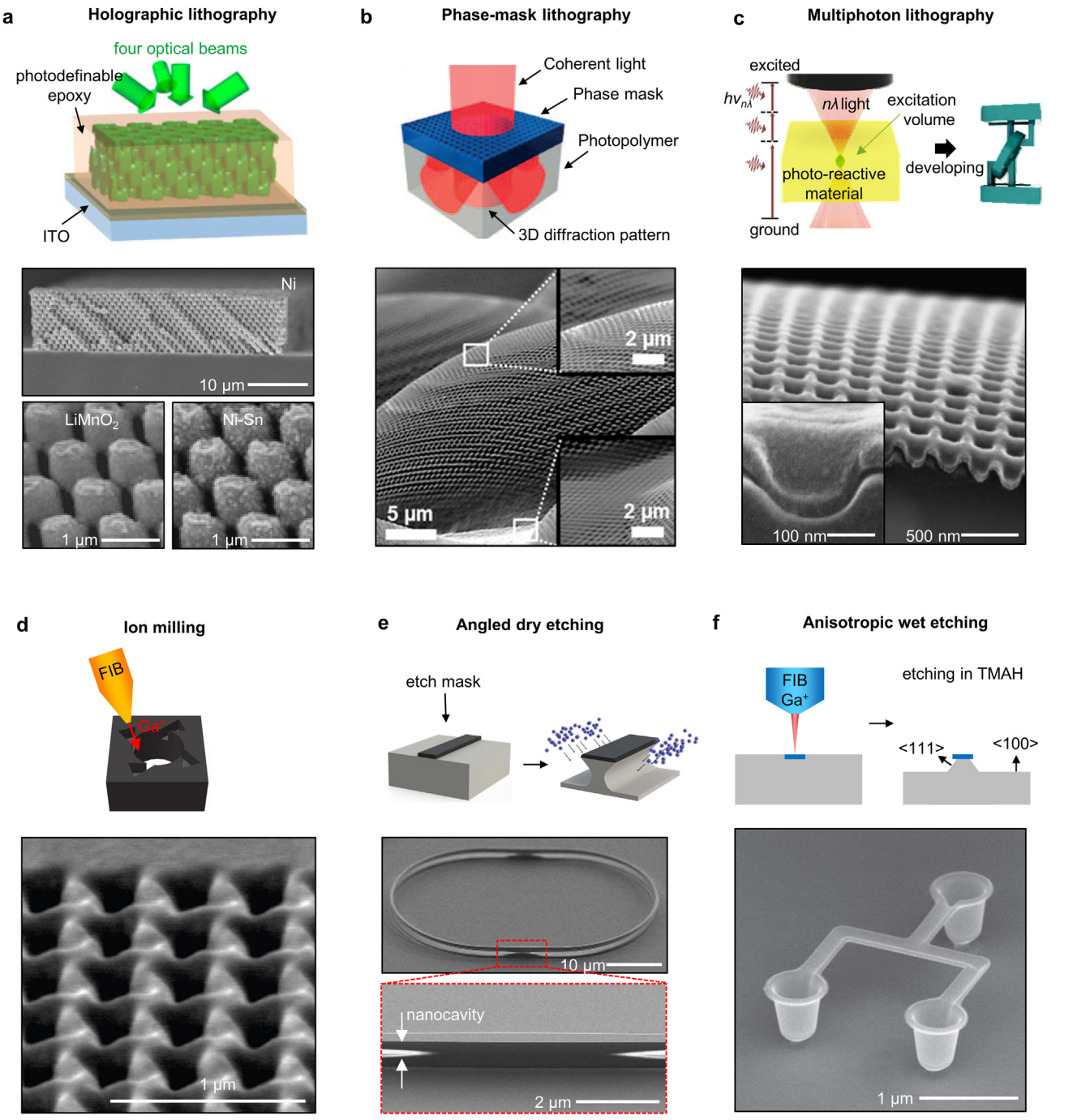

Fig. 1. Top-down approaches for the fabrication of functional 3D nanostructures. a) Schematic illustration (top) and SEM images (bottom) of 3D nanostructured anodes and cathodes fabricated by holographic lithography. Adapted with permission from National Academy of Sciences [14]. b) Schematic illustration (top) and SEM images (bottom) of 3D hierarchical photonic nanostructured surfaces fabricated by phase-mask lithography. Adapted with permission from Wiley-VCH [109] and American Chemical Society [115], respectively. c) Schematic illustration (top) and SEM images (bottom) of 3D plasmonic surfaces fabricated by multiphoton lithography and nanoimprint. Adapted from [125]. d) Schematic illustration (top) and SEM image (bottom) of 3D chiral structure arrays formed by FIB milling. Adapted from [141]. e) Schematic illustration (top) and SEM images (bottom) of a 3D structure with nanocavity in bulk single-crystal diamond fabricated by angled dry etching. Adapted with permission from Springer Nature [17]. f) Schematic illustration (top) and SEM image (bottom) of a 3D nanostructure in silicon fabricated by ion implantation and anisotropic wet etching. Adapted with permission from IOP Publishing [155].

of technique can create 3D nanoscale features without the use of complex optical systems, photomasks or multiple processing sequences. Here, an interference pattern generated by spatial and temporal overlap of coherent light waves in 3D space exposes light-sensitive materials that yield, upon development, corresponding solid structures [99–101]. As an example, holographic lithography can create 3D nanostructures in $LiMnO_2$ and Ni-Sn for high-performance Li-ion microbatteries [14]. The fabrication process involves four interfering laser beams arranged in an umbrella geometry [102] to create a 3D lattice structure in a photodefinable epoxy (SU-8) with a periodicity of ~1 μm and a porosity of ~40% (Fig. 1a, top part). Adjusting the polarization, intensity and angle of each beam in this setup provides access to various nanostructures with feature sizes down to ~10 nm [103]. Resulting 3D nanostructures in epoxy can serve as templates for further integration of functional materials as anodes and cathodes for lithium-ion

microbatteries. Specifically, electroplating thick layers of Ni can fill the gaps in these types of 3D nanostructures. Removing the epoxy leaves 3D nanostructures in Ni, with inverted 3D geometries (Fig. 1a, middle part). Subsequent pulse electroplating of Ni-Sn and MnO_2 on the surface of the Ni forms anodes and cathodes, respectively. $LiNO_3$/LiOH molten salt then lithiates the electrolytic MnO_2. Scanning electron microscope (SEM) images of 3D nanostructures of $LiMnO_2$ and Ni-Sn appear in Fig. 1a (bottom part). Li-ion microbatteries based on these materials exhibit high energy (6.5 μWh cm^{-2} μm^{-1}) and peak power (3600 $\mu W\ cm^{-2}$ μm^{-1}) densities, due primarily to the large surface areas of these systems. Holographic lithography in this case not only provides routes to achieving such types of anodes and cathodes, but also offers flexibility in tuning the tortuosity and porosity of the structures, both of which have important additional roles in defining the performance attributes of the batteries [104,105]. In addition to energy storage devices as highlighted in this example, other applications of 3D functional nanostructures formed by holographic lithography include optical biosensors [106], microfluidics [107], and optical metamaterials with negative refractive index [108].

The creation of light interference in 3D space can alternatively be realized through the use of phase masks with features of relief that have dimensions comparable to those of the optical wavelength. Placing such a mask into conformal contact with a photosensitive layer followed by flood exposure leads to the generation of complex, but well-defined 3D patterns of light within the material. Subsequent development yields 3D nanoscale features across large areas in a simple process (Fig. 1b, top part) [85,109–111]. This form of 3D nanoscale patterning, sometimes referred to as proximity-field nanopatterning, typically uses soft, elastomers for the phase masks [109] or collections of colloidal nanospheres [112–114]. The 3D structure geometries depend on the mask design, wavelength, polarization and coherence of the exposure light, and the optical properties of the photosensitive material. This method can form a wide variety of 3D periodic and quasi-periodic nanostructures such as woodpile structures and quasicrystal systems, with feature sizes as small as 50 nm. 3D nanopatterning using phase masks requires much simpler optical setups and reduced light coherence as compared to multibeam holographic lithography. Demonstrated utility of nanostructures fabricated by this method include biomimetic hierarchical photonics (Fig. 1b, bottom part) [115], substrates for Raman analysis [116], stretchable electronics [117], and gas sensing [118]. Additionally, 3D photopolymer nanostructures can serve as templates for the coating of metal oxides or other materials for applications in nanofluidics [119], optical metamaterials [120], and functional nanocomposites [121].

Other light-based techniques such as multiphoton lithography with a scanning beam provide access to 3D structures with nearly arbitrary shapes and feature sizes across a wide range of dimensions down to tens of nanometers [80,122]. A key feature is that the nonlinearity of the process allows patterning into the depth of a photosensitive material by scanning the position of a tightly focused spot (Fig. 1c, top part). In many cases, 3D nanostructures formed in this way rely on specialized polymers with strong two-photon absorption cross sections, typically at infrared wavelengths. Often these polymers serve as sacrificial templates for the growth or deposition of other materials, or as masters for molding or for imprinting. The latter operates in a parallel fashion over large areas [95] and is compatible with both rigid and flexible substrates [123,124]. Fig. 1c (bottom part) shows an SEM image of a 3D periodic nanostructure in epoxy coated with aluminum, formed by imprinting using a master created by multiphoton lithography [125]. This particular type of nanostructure has applications in plasmonics [126,127]. Moreover, incorporation of high-birefringence liquid crystals in these nanostructures serves as the basis for an unusual optical modulator with a full range of dynamically tunable color spanning the entire visible region of the spectrum, with potential applications in filters, reflective displays, and other optical devices [128–131].

Most such techniques start with patterning of photosensitive polymers into 3D nanostructures. Forming structures in metals, ceramics and other materials occurs through conformal deposition and selective removal of the polymer [88]. As described above, these structures can also serve as templates for infilling or imprinting to yield 3D systems with inverse geometries in other materials [125,132,133]. Direct lithography can be performed using photosensitive chemistries that contain functional components or groups, such as metal-rich composite photoresists [83,134,135], photoresists that embed piezoelectric nanoparticles [77], and chalcogenides [136], to further broaden the classes of materials, with demonstrated utility in 3D MEMS, battery electrodes, cell scaffolds, and others [77,83,134]. While these and other options are valuable, many classes of materials cannot be patterned in this way due to temperature limitations, difficulties in crystal growth or other constraints.

Etching-based techniques that selectively remove materials serve as important alternatives in this context. Here, removal of bulk or thin-film materials relies on exposure of materials to two basic types of etchants: plasma-phase (dry etching) and liquid-phase (wet etching). Fabricating 3D nanostructures in this manner typically requires both nanoscale etching resolution and anisotropy in the etching direction.

Dry etching occurs through either a physical or chemical process. Ion milling, or sputter etching, is a physical process that is well-suited for fabricating 3D nanostructures in various materials. Ion milling typically employs a focused ion beam (FIB) typically of gallium that removes material from the surface of a sample, to a desired depth. A highly focused beam can support a resolution down to 10 nm with large etching anisotropy in the direction of the beam. Adjusting the angle of the beam with respect to the sample surface enables milling in 3D space (Fig. 1d, top part), accompanied by in-situ imaging capabilities using a separate electron beam in a dual beam FIB configuration. This type of 3D nanomachining process is effective with different classes of materials including metals [137], semiconductors [138], dielectrics [139], and biomaterials [140], largely due to the physical nature of its operation. Fig. 1d (bottom part) shows an example of a 3D hole array structure formed in a gold film by 3D ion milling [141]. Such metal-based sophisticated 3D photonic nanostructures could be useful as chiral metamaterials with large optical activity [142,143]. Despite the advantages of ion milling in fabrication precision and applicability to different materials, there are distinct drawbacks of this method such as slow milling speeds, requirements for vacuum conditions, potential surface damage and undesired implantation of ion impurities.

By contrast to this type of physical manipulation, chemical dry etching processes involve reactions of materials with gas phase species. Typical methods such as reactive ion etching generate 2D structures through an etching mask as a result of the vertical etching directionality. When combined with angled chemical dry etching, however, the results can yield 3D nanostructures in functional materials [16,17,144]. For example, fabrication of the 3D nanostructure shown in Fig. 1e [17] first exploits electron beam lithography and plasma etching techniques to yield an etching mask in silica. Subsequent oxygen plasma etching of single-crystal diamond at an oblique angle (~50°) yields a suspended racetrack structure with nanocavities (~500 nm in feature size). This system forms a nanophotonic resonator with large optical quality factor ($>10^5$) and operating wavelengths that span the visible and telecom regimes of the spectrum. Altering the layouts of the etching masks and the etching directions provides access to other 3D nanostructures such as nano-rings, straight and spiral nano-beams [144], with potential applications in non-linear optics, chemical sensing,

and others. Additional advances in dry etching of 3D nanostructures include simultaneous multi-directional plasma etching of single-crystalline silicon as photonic crystals with high reflectance (> 95%) and low transmittance (<-15 dB) at optical communication wavelengths [145].

Wet etching, especially anisotropic wet etching, is a well-established approach to fabricating 3D nanostructures in semiconductor materials such as device-grade silicon and III-V compound semiconductors, with wide applicability in microelectronics, optoelectronics and MEMS [146,147]. Two common etchant systems for anisotropic wet etching of silicon are ethylenediamine-pyrocatechol-water solutions [148,149], and inorganic alkaline solutions such as KOH, NaOH, and tetramethylammonium hydroxide (TMAH) [150,151]. For both chemistries, the etching rates depend on the doping levels [152–154]. A variety of 3D nanostructures are, therefore, achievable through the use of selective nanoscale doping as masks for subsequent wet etching. Results in Fig. 1f exploit gallium ion implantation by FIB to yield doping patterns in silicon with nanoscale resolution [155]. Specifically, Ga-doped p^+ silicon serves as an etch stop with a depth up to several microns during etching with TMAH [156]. Here, selective dissolution of (100) silicon in the preferential <111> plane, in combination with spatial masking using ion implantation, can yield sophisticated 3D nanostructures with overhanging features. To avoid defects created by ion implantation, a combination of atomic layer deposition (ALD) and FIB milling can yield separate masks for anisotropic wet etching [157]. The diversity of achievable geometries in semiconductor materials with minimal damage to their electrical properties suggest opportunities for applications of such nanostructures in nanoelectronics and nanophotonics.

Bottom-up techniques

The top-down methods described in the previous section provide exceptional levels of engineering control, but they require complex tools, multiple processing steps, and have narrow processing tolerances. Furthermore, these schemes do not typically apply well to soft or chemically/thermally fragile materials such as organic semiconductors, biomolecules, and living systems. As alternatives, bottom-up strategies are appealing because they rely on processes governed by thermodynamics or kinetics such as self-assembly, materials growth, chemical synthesis, and/or deposition of atoms, molecules, or particles [158–160]. Although such strategies typically provide modest levels of control over geometric parameters, they can support high throughput due to the parallel, and sometimes volumetric, nature of the underlying operation. Current research focuses on means to adapt such processes for modern manufacturing of functional 3D nanomaterials and nanostructures. This section reviews some of the latest advances, with an emphasis on functional structures and systems.

One of the most attractive bottom-up routes involves the self-assembly of nanoscale building blocks to form organized 3D nanostructures according to the rules of interactions among themselves, without external application of guiding forces. Such building blocks include colloids [161,162], DNA [163], domains in block copolymers [164], and many others [165,166]. For example, the self-assembly of block copolymers provides a straightforward path to 3D nanoscale objects [23,167,168]. Here, phase separation of the copolymers into various morphologies depends on the polymer architectures and their relative volume fractions [169], to yield constructs that include lamallae, gyriods, cylinders, and spheres [170]. Previous publications describe formation of 3D functional nanostructures in this manner, with demonstrations in photovoltaics [171], electrochemistry [172], and optics [173]. Recent research focuses on the use of block copolymer templates to guide the formation of other 3D nanostructures. For example, block copolymers that have a crystallizable core-forming block can act as precursors to form triblock comicelle building blocks in the forms of either H (hydrophobic)-P (polar)-H or P-H-P comicelles, by the addition of unimers to a solution of monodisperse cylindrical block copolymer micelles (Fig. 2a, top part) [167]. These nanoscopic components can form a wide variety of superstructures through end-to-end intermicellar stacking, and the process is readily controllable by selecting the comicelle architecture and the solvent used. Fig. 2a (bottom part) presents a complex 3D network formed by adding decane to a solution of P-H-P triblock comicelles. Such assemblies possess multiple levels of structural hierarchy and they can exist over length scales of several microns. Other examples of block copolymer-templated fabrication of functional materials include metal (e.g. gold, nickel) for optical and photonic applications [174,175], iron oxide for sensing [176], and silicon for optical anti-reflection [177].

As a form of molecular self-assembly, DNA-based techniques offer additional routes to the formation of nanoscale 3D structures. DNA is a unique building block material in this context because of its well-defined chemistry, mechanical flexibility, and ability to fold [178–181]. Base-pairing rules allow for deterministic design of complex 3D nanostructures. DNA origami is the most prominent example of this form of self-assembly, where a self-folding process involving a long single-stranded piece of DNA transforms into a prescribed 2D or 3D structure by short DNA oligonucleotides complementary to specific regions of the scaffold DNA [182,183] (Fig. 2b, top part). These 3D DNA origami constructs can serve as templates for the growth of other materials in 3D forms.

A limitation is that such structures require high-ionic-strength solutions to maintain their geometries, which results in surface charging that can oppose the deposition of materials due to electrostatic forces. A recently developed modification of the Stöber method [184], a sol-gel process for preparing silica particles, allows for deposition of silica nanostructures on 3D DNA origami templates [25]. The approach relies on optimizing the synthesis conditions that lead to cluster formation of mineral precursor molecules rather than deposition directly on the DNA backbones. The cluster formation, promoted by an intermediate step for pre-hydrolysis, forms an inductive layer around the DNA origami structures, facilitating subsequent silica deposition. This strategy enables accurate 3D shape replication from DNA origami templates to DNA-silica composites with a wide range of shapes, with sizes spanning from 10 to 1,000 nm. Fig. 2b (bottom part) presents designed models and corresponding TEM images of 3D DNA origami templates and deposited silica nanostructures [25,185].

Other efforts are in the assembly of larger 3D DNA structures through the assembly of DNA bricks consisting of four short binding domains for interlocking [186]. Recent progress in this direction includes the assembly of complex, programmed 3D nanostructures from tens of thousands of unique components, which is made possible by use of DNA bricks with longer, 13-nucleaotide binding domains [187]. Even larger 3D DNA structures might be possible with further optimization of the 3D assembly process, for potential applications such as positioning functional components.

In addition to these and related assembly-based methods, liquid and vapor-phase deposition techniques provide additional options in direct access to 3D nanostructures, typically used in combination with material templating or patterning. Vapor-phase schemes include chemical and physical vapor deposition (CVD and PVD, respectively). CVD methods typically involve chemical reactions of gaseous reactants activated by heat, light or plasma, resulting in self-assembled growth at the molecular level in 1D or 2D formats. Direct CVD growth of 3D structures is achievable, for example, via local strain engineering. One example is the direct synthesis of freeform 3D micro/nano carbon nanotube structures by locally

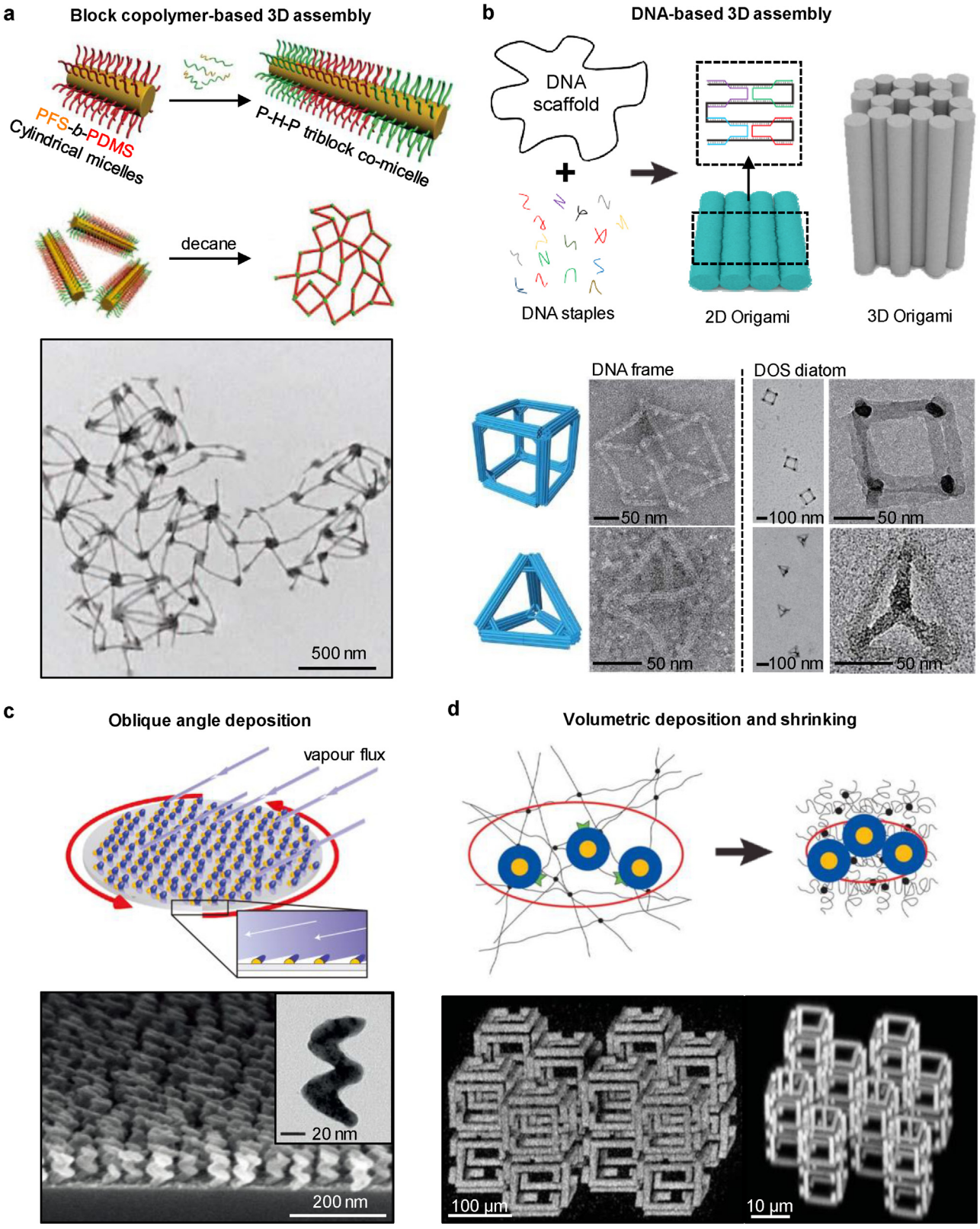

Fig. 2. Bottom-up approaches for the fabrication of functional 3D nanostructures. a) Schematic illustration of the process for assembly of 3D superstructures through stacking of triblock co-micelles (top) and TEM image of an irregular network of superstructures formed by this process (bottom). Adapted with permission from AAAS [167]. b) Schematic illustration of DNA origami design strategies for 2D and 3D objects (top). Adapted with permission from Elsevier [182]; design models and corresponding TEM images of DNA origami templates, and 3D silicification of diatom nanostructures (bottom). Adapted with permission from Springer Nature [25]. c) Fabrication illustration (top) and SEM image (bottom) of arrays of Ag:Cu alloy helices formed using physical vapor deposition at grazing incidence. Adapted with permission from Springer Nature [26]. d) Schematic illustration of the volumetric deposition and shrinking process showing silver (blue) on top of gold nanoparticles within a hydrogel matrix (top); maximum-intensity projection of a reflected light image of a 3D structure that follows from volumetric silver deposition prior to shrinking (bottom, left) and a fluorescent image of the same structure after shrinking (bottom, right). Adapted with permission from AAAS [198].

modulating growth rates to induce curvature of the structures [188–190]. PVD methods involve vaporization of source materials with beams of electron, ions or photons followed by solidification on target substrates. Glancing angle PVD provides quick and efficient access to complex 3D nanostructures [191–194]. As an example, a glancing angle deposition (GLAD) process for fabricating 3D nanocolloids starts with the formation of an array of nucleation sites on a substrate, followed by deposition of a desired material at a glancing angle (Fig. 2c, top part) [26]. The dimensions and shapes depend on the patterns of nucleation sites, the substrate tilt and rotation, and the deposition conditions. Achievable structures include columnar rods, zigzag structures, twisted and helical forms with feature sizes as small as 20 nm, applicable to multiple functional materials including Ag, Cu, Ti, Ni, Si, Al_2O_3, and TiO_2. Sequential deposition and co-deposition of materials enable hybrid and alloy nanostructures, respectively. Fig. 2c (bottom part) shows SEM and TEM (inset) images of 3D Ag:Cu alloy helices grown on a wafer by co-deposition via GLAD from two evaporation sources. Control over the shape and composition enables their use as plasmonic metamaterials, such as plasmonic chiral light antennas with tunable chiroptical properties [73,195,196]. Limitations of this approach lie in the difficulty in forming complex structures such as those involving looped shapes, knots or branched structures, as well as the requirements for materials compatibility with vacuum conditions.

Deposition-based techniques combined with volumetric shrinking support additional access to 3D materials at the nanoscale [197,198]. A recent example involves the direct assembly of 3D nanomaterials in arbitrary geometries by volumetric deposition in the liquid phase followed by controlled shrinkage of the patterned scaffolds [198]. The process uses polyacrylate hydrogel scaffolds formed using two-photon lithography, with fluorescein molecules attached to predefined locations in the gel through reactions induced by two-photon excitation, to act as anchors for the deposition of functional molecules and nanoparticles using conjugation chemistries. Subsequent shrinking of the patterned and functionalized gel scaffold by a factor of 10–20 yields the desired nanoscale resolution, by using acid or divalent cations to dehydrate the gel (Fig. 2d). The modular nature of the assembly process allows for a range of materials to be deposited, including metals, semiconductors, and biomolecules, although corresponding aqueous deposition chemistries are necessary. Independent control over the geometry and composition of this method suggests opportunities for the use of these 3D functional structures in nanophotonics, metamateirals, and plasmonics.

Guided assembly

Recent work demonstrates that structures in 2D formats can be geometrically transformed into 3D architectures by processes that occur within the structures themselves or through their supporting substrates. Such processes enable the formation of 3D structures with nanoscale thickness or lateral dimensions. These processes offer significant design versatility, ranging from simple curved structures that result from relaxation of residual stresses in thin films to complex, hierarchical 3D platforms that support high performance electronic and optoelectronic devices [29,199,200]. This section classifies such methods according to the nature of the driving forces for 2D to 3D shape transformations: a) residual stresses, b) external stimuli, and c) substrate deformation.

Transformations driven by residual stresses

The release of thin films formed with gradients of residual stress on planar substrates leads to the spontaneous formation of deformed micro- and nanostructures with geometries determined by the thicknesses of the films, the magnitudes of the stresses, and the 2D geometries of the released areas [27,201,202]. Methods to generate residual stresses in thin films for these purposes fall in two main categories: intrinsic stresses created during thin film growth or deposition, and other stress-inducing mechanisms such as lattice mismatch, thermal stress, energetic deposition, and ion beam irradiation [203,204]. Both mechanisms are often operative. The following paragraphs discuss the methods and examples of their use in 3D nanostructure formation.

Intrinsic stresses are related to the kinetic processes of thin film growth or deposition, which occur under non-equilibrium conditions. Compressive or tensile stresses may originate from microstructure evolution such as insertion of atoms at grain boundaries and grain boundary growth [203]. The polarity and magnitude depend on the deposition techniques and conditions. Common methods include thermal and electron beam evaporation, CVD, and ALD. A stack of sequentially deposited films with different intrinsic stresses can roll up into curved or tubular structures once released from substrates, typically through elimination of a sacrificial layer (Fig. 3a, left) [205]. This stress-induced curling applies to almost all types of thin film materials and deposition conditions, including metals, semiconductors, and dielectrics. This versatility, taken together with compatibility with planar lithographic processes, can be exploited to allow for the creation of 3D functional devices. Recent examples include 3D rolled-up nanomembranes for energy storage devices [206], photodetectors [207], optical resonators [208], soft electronics [71], and gas sensors [209]. In many cases, the 3D, multilayer tubular configuration provides advantages over planar membranes, as exemplified by a 3D radio-frequency transformer consisting of multiple layers of nanoscale membranes to achieve large coupling coefficients and high maximum working frequencies compared to those of devices that use planar designs (Fig. 3a, middle) [210]. In addition to basic tubular structures, various other self-rolling geometries are also achievable by patterning the nanomembranes, including jagged ribbons, rings, and helices (Fig. 3a, right) [28,211].

In addition to intrinsic stresses related to growth kinetics, other mechanisms can also be relevant. For example, differences in crystal structure or lattice parameters between crystalline thin films and underlying materials may give rise to residual stresses, known as epitaxial stresses. Tensile strain develops when the equilibrium lattice constant of the film is smaller than that of the underlying material, and compressive strain develops for the opposite case (Fig. 3b). Heteroepitaxial crystalline bilayers with tensile strain in the top layer and compressive strain in the bottom layer can bend upwards and form rolled-up structures upon release. Typical examples of such heteroepitaxial bilayer materials systems include GaAs/InAs [212], InGaAs/GaAs [213], SiGe [31], AlN/GaN [214], and GeSn/Ge [215]. Recent progresses in lattice mismatch-induced rolling include predictive engineering of membrane geometry to achieve controlled, unidirectional roll-up [216] and rolled-up nanomembranes as high electron mobility transistors [217] and terahertz metamaterials [218].

Differences in the coefficient of thermal expansion (CTE) of the film and the substrate can serve as another source of residual stress in thin films. Such stresses have magnitudes that are proportional to the change in temperature and the difference between the CTE values of the thin film and the substrate [219,220]. Utilization of the large thermal stresses enables the fabrication of nanoscrolls of various functional materials including transition metal dichalcogenides (TMDs) and TMD-based hybrids (Fig. 3c) [221]. As an example, the cooling of monolayer TMD flakes grown on SiO_2/Si substrates at high temperatures (> 700 °C) to room temperature introduces thermal stresses in the flakes. Subsequently, release of the thermal stresses through the insertion of liquid between the TMD flakes

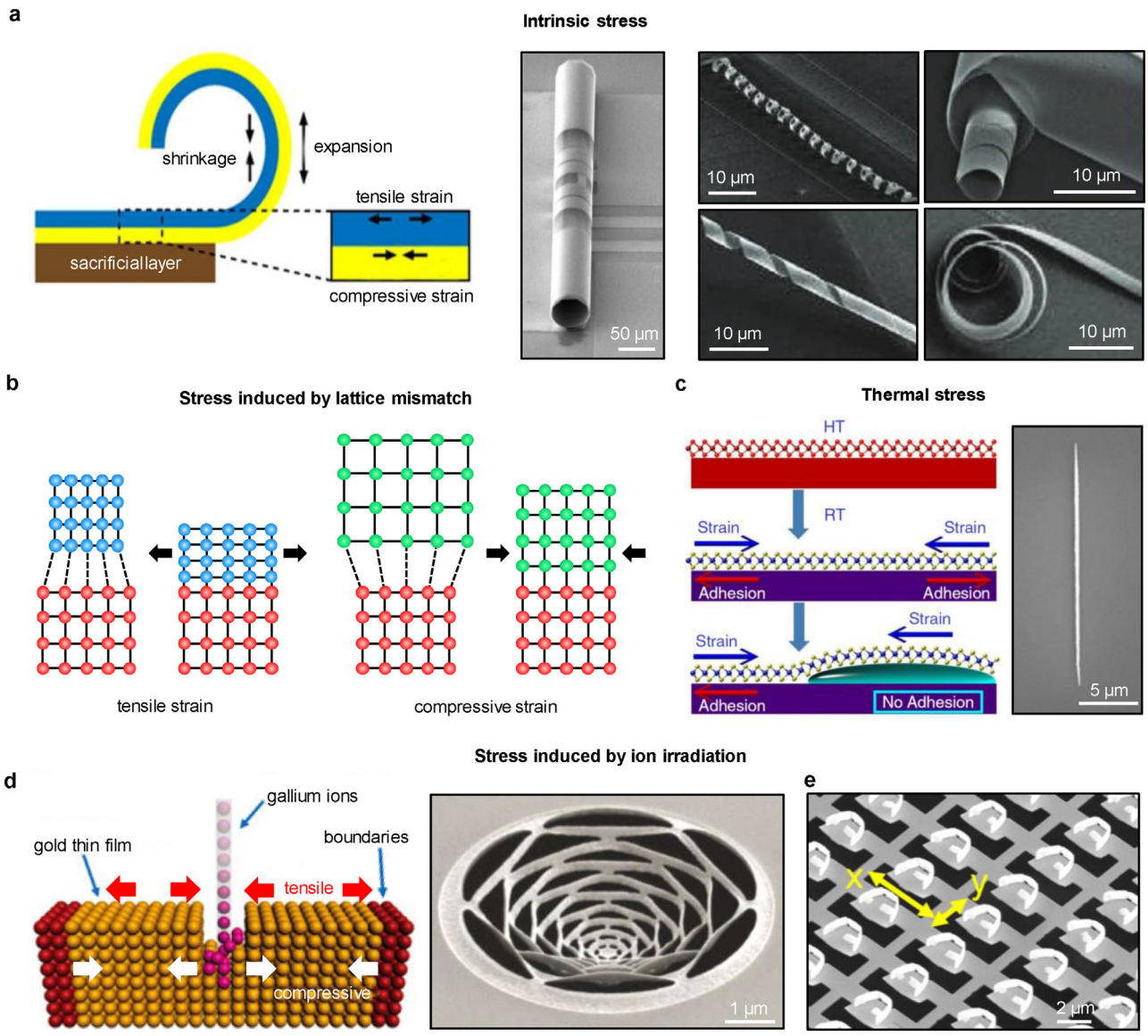

Fig. 3. Guided assembly of functional 3D nanostructures by internal forces. a) Rolling of a nanomembrane due to release of intrinsic stress after selective etching of a sacrificial layer (left). Adapted from [205]; SEM image of a self-rolled-up multilayer nanomembrane as a radio-frequency transformer (middle). Adapted with permission from Springer Nature [210]; SEM images of 3D diamond nanomembranes formed by internal strain-induced rolling and twisting (right). Adapted with permission from Wiley-VCH [28]. b) Scheme showing built-in internal strain developed due to heteroepitaxial growth (left); c) Scheme (left) and SEM image (right) of MoS_2 nanoscrolls on SiO_2/Si substrates formed by thermal stress-induced rolling. Adapted from [221]. d) Schematic illustration of FIB-induced internal stress in gold thin films (left) Adapted from [223]; SEM images of a spider web-like gold thin film structure after ion beam irradiation (middle). Adapted with permission from AAAS [13]; SEM image of a multi-direction-tunable 3D Si_3N_4/Au metasurface (right). Adapted with permission from American Chemical Society [225].

and the substrate leads to the out-of-plane curving of the monolayer flakes into nanoscrolls. The 3D self-encapsulated structure gives rise to optical and electronic properties that are more stable and insensitive to ambient conditions, as compared to their 2D counterparts.

Ion beam irradiation is another means for inducing residual stress in thin films, in a highly controlled manner. Here, FIB irradiation creates local stresses or forces in thin film materials, enabling complex deformations of films into 3D structures. The utility for forming 3D nanostructures follows from this nanoscale spatial resolution of FIB and its applicability to various metals and dielectric thin films [222]. In one example, irradiation of gallium ions on gold films (~ 20 nm thick) causes well defined distributions of residual stress, including tensile stresses near the film surface due to gold grain coalescence and compressive stresses underneath the surface due to gallium ion implantation (Fig. 3d) [13,223,224]. These stress variations through the film thickness can yield local bending or twisting, depending on the pattern and constraints of the thin films. FIB irradiation at high doses can cut through thin films. This local cutting process, in combination with global ion irradiation, enables 3D nanoscale “kirigami” to form rich varieties of 3D shape transformations such as upward buckling, downward bending, complex rotation, and out-of-plane twisting [13]. 3D helical or pinwheel-like structures formed by this method exhibit large optical chirality [13]. Using a similar fabrication technique, metasurfaces composed of an array of 3D nano split-ring-resonators show reversible and large-range changes of optical characteristics in infrared regime (Fig. 3e) [225,226]. The process for forming each 3D split-ring-resonator involves cutting and multiple steps of local irradiation-induced bending.

Transformations driven by external stimuli

In the previous section, the formation of 3D nanostructures mainly occurs due to the release of residual stress of films developed during or after deposition, or through ion irradiation. Alternatively, external stimuli associated with exposure to heat, light, liquids, or changes in pH can generate forces and cause local deformation or assembly of materials to form 3D geometries, thereby providing additional routes to triggering 2D to 3D shape transformations.

One example is capillary forces, which are particularly attractive for triggering self-assembly of materials into 3D nanostructures because of the favorable scaling effects at micro/nano dimensions. Capillary self-assembly provides a simple and scalable route to forming 3D nanostructures, typically from 1D (e.g. wires, pillars) or 2D planar structures. Fig. 4a illustrates this type of process where micro/nanoscale photopolymer vertical pillars produced by femtosecond laser polymerization assemble into 3D hierarchical architectures by capillary forces [227]. The schemes start with immersing nanoscale pillars with arbitrary 2D patterns in a solvent. Evaporation of the solvent induces capillary forces, which bend pillars into 3D configurations. Van der Waals forces at the areas of contact between bent pillars cause retention of the bent configurations after solvent evaporation. By designing the 2D pattern and controlling the evaporation process, diverse 3D micro- and nanostructures in large arrays can be achieved. Demonstration of the use of these 3D hierarchical micro- and nanostructures for selective trapping and releasing of microparticles suggests their potential applications in microfluidic systems and biomedicine [228,229].

Another related driving force arises from surface tension associated with liquid evaporation [230] or material melting. In the latter context, FIB is a commonly used source of highly localized heat for melting of polymers [231,232] or metals [233]. Fig. 4b shows an example where surface tension forces generated by melting of a polymer (poly(methyl methacrylate)) lead to folding of an origami-inspired structure into a 3D nanocage geometry [232]. Localized heat generation triggered by FIB irradiation raises the temperature of the planar polymer hinges above their glass transition temperature, generating surface tension forces toward the center of the polymer hinges. These forces induce folding of the surrounding panels. 3D cubic split-ring resonators with polymer hinges fabricated by this method offer interesting opportunities in 3D optics such as metamaterials with negative index of refraction and significantly reduced losses in frequency spectrum over similar devices with metallic hinges.

Heating-induced shape change of thermally responsive materials is another commonly used strategy to trigger 3D self-assembly. Such materials include certain hydrogels, shape memory polymers, liquid crystal polymers, and composite materials containing thermally responsive components. These materials can be incorporated into thin films to provide thermally-driven, 2D to 3D shape transformations to form structures with key dimensions in the nanoscale regime. Fig. 4c shows one such example where monolayer graphene functionalized with thermoresponsive polymers folds into 3D flower shapes upon heating to 45 °C from room temperature, and unfolds upon cooling [234]. Functionalization of the graphene starts with the surface, self-polymerization of dopamine to form a thin layer of polydopamine, which allows the grafting of a thermoresponsive polymer poly (*N*-isopropylacrylamide) (PNIPAM). Lithographic patterning of the functionalized graphene defines the sizes and shapes of the 2D precursors. After release from a sacrificial layer and heating above the lower critical solution temperature of the PNIPAM, the 2D precursors self-fold into well controlled 3D microstructures with thicknesses of 5−10 nm. This approach provides access to manipulation and folding of chemically inert graphene sheets into 3D geometries via non-covalent surface functionalization, without altering the intrinsic properties of the graphene. Such systems can be used to encapsulate live cells and to form unusual classes of transistor devices [234,235].

In addition to heat, other external stimuli such as those due to changes in ion concentrations can also actuate the transformation of planar graphene sheets into 3D structures. For example, a recent study describes the formation of various origami-inspired 3D structures using a bimorph composed of graphene and a 2 nm-thick patterned layer of glass [236]. The graphene-glass bimorph can bend in response to local electrolyte concentration due to an ion exchange reaction within the glass, causing the glass to swell relative to the graphene. This bending can be designed to occur in specifically designed regions through the use of patterns of photoresist on the bimorph to prevent bending beneath them. The degree of local bending depends on the geometry of the bimorph and the pH of the surrounding environment. The scheme enables the fabrication of 3D microstructures including tetrahedrons (Fig. 4d), helices, cubes and others. These graphene-based microscale structures can sense the environment and perform shape morphing on time and length scales comparable with biological organisms. Potential incorporation of electronic and photonic devices into these 3D systems may yield applications in microscale robotics.

Transformations driven by substrate deformations

3D structures formed by the release of internal strain or external stimuli are limited to basic shapes created by bending/folding/rolling in a specific direction largely depending on the materials used. Therefore, the types of 3D geometries achievable using these methods are limited. Moreover, the shape transformation mechanisms depend critically on material properties, thereby significantly limiting their applicability to a broad range of functional materials such as device-grade semiconductor materials. A relatively recent set of mechanically guided compressive buckling techniques [53,237] avoid these constraints, to offer broad ranging material compatibility, fabrication scalability, design versatility, and the high level of process control. These processes start with patterning thin film materials in planar formats (referred to as “2D precursors”) using any of the most advanced microfabrication techniques, followed by defining specific regions on these 2D precursors to bond with a pre-stretched elastomeric substrate through patterned surface functionalization. Release of the prestrain in the substrate imparts compressive forces to the 2D precursors through the bonding sites, thereby transforming them into well-controlled 3D structures through spatially dependent in- and out-of-plane translational and rotational motions. The targeted 3D shapes can be controlled by the design of the 2D precursor, the thickness and mechanical properties of the materials in the 2D layout, the size and shape of the bonding sites, and the prestretching applied to the elastomeric substrate. The choices of these parameters for targeted 3D shapes can be guided with high accuracy, by quantitative, finite element modeling [68,238–240]. Since the assembly process follows from nonlinear buckling mechanics, this method applies intrinsically to almost all types of materials including metals, polymers, semiconductors, 2D materials, thermoelectric and piezoelectric materials [6,241–243]. The scaling of the buckling mechanics also makes this method applicable to a broad range of length scales, from nanometer to centimeter and even meter scale dimensions [244]. Furthermore, various structural design strategies allow for the realization of complex 3D architectures that are otherwise challenging to fabricate using other methods, including origami- and kirigami-inspired structures [57,245], multilayer structures [246], morphable structures [247], and out-of-plane chiral structures [248]. The following para-

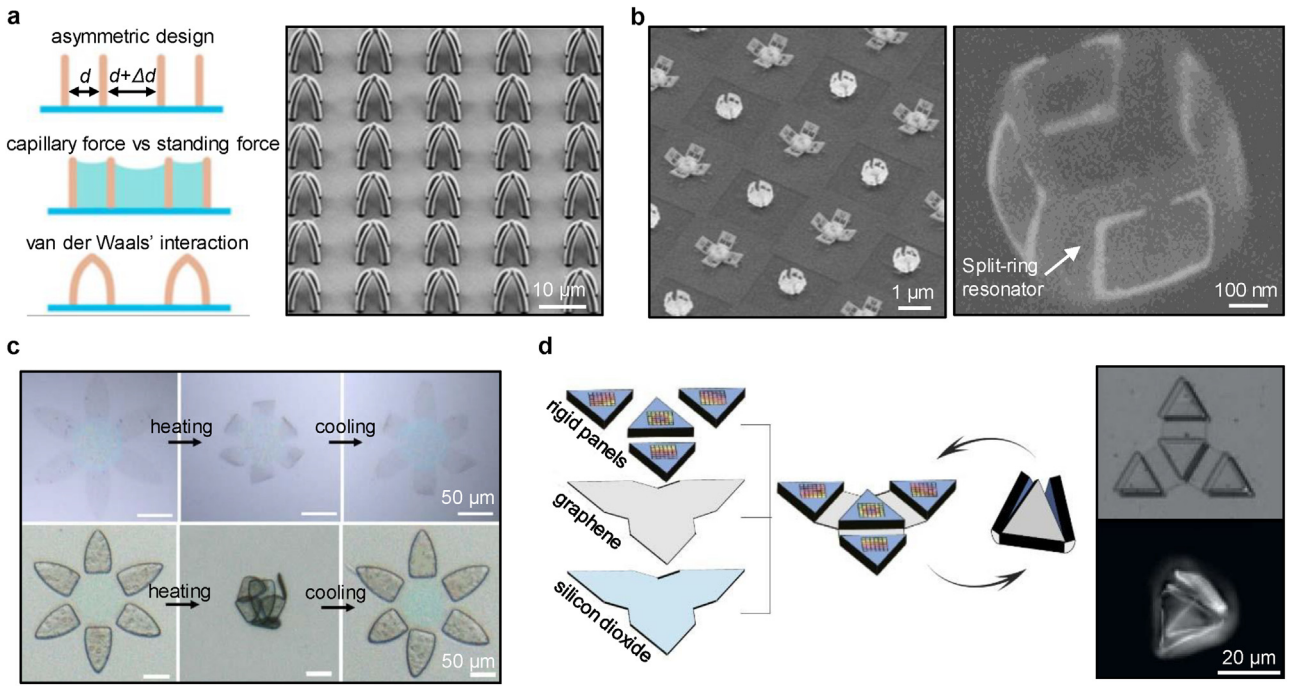

Fig. 4. Guided assembly of functional 3D nanostructures by external forces. a) Schematic illustration and SEM image of 3D nanopillars assembled by capillary forces. Adapted with permission from National Academy of Sciences [227]. b) SEM images of cubic resonators assembled by capillary forces during ion-induced localized polymer reflow. Adapted with permission from American Chemical Society [232]. c) Optical image of heat-induced self-folding of functionalized graphene (top) and SU-8/graphene (bottom). Adapted with permission from AAAS [234]. d) Scheme of the formation of a 3D cube made of graphene-glass bimorph by self-assembled folding in response to heat or electrolyte concentration (left) and SEM images of graphene-glass bimorphs before and after folding into a tetrahedron (right). Adapted with permission from National Academy of Sciences [236].

graphs summarize some recent progress in constructing functional 3D structures and devices using this method.

A relevant example is in the assembly of an array of photodetectors comprising MoS_2 and graphene as photoactive and electrode layers supported by a photodefinable epoxy (SU-8), into 3D hemispherical structures capable of real-time light imaging with measurements of the direction, intensity and angular divergence properties [6]. Fig. 5a shows the key fabrication steps involved in transforming the system from a 2D precursor into a 3D hemispherical shape. Removal of the precursor from a temporary substrate and subsequent attachment to a pre-stretched elastomer substrate yields, upon release of the prestrain, the desired 3D geometry, with high precision. Related geometries including octagonal prisms, octagonal prismoids, and hemispherical domes are also possible. The maximum strain adopted by the active layers, graphene and MoS_2 during the 2D to 3D shape transformation remain well below their fracture levels of 6% and 2%, respectively [249–254]. Graphene electrode lines connect the MoS_2 photodetector, forming a photodetector unit cell on the 3D hemispherical platform (Fig. 5b). The passage of a laser beam through this transparent (~87% transmittance at 550 nm) system provides information about the entry and exit, thereby allowing real-time mapping of the intensity and direction of the incident light (Fig. 5c). Such capability follows uniquely and naturally from the 3D architecture, with no simple analog in conventional planar systems. Such systems can be formed simultaneously, in large arrays and with dimensions and levels of integration beyond those illustrated here.

3D micro- and mesostructures formed by this method can serve as templates for the formation of functional nanostructures in 3D architectures with unique optical and electronic properties. An example uses 3D Si-SiO_2 structures for high-temperature templated growth of AgCl-KCl eutectics [65]. The process starts with the formation of a 3D Si-epoxy cage structure using compressive buckling, followed by transfer of the 3D structure onto quartz or Si substrates with a thin adhesive layer of polydimethylsiloxane (PDMS). Next, conformal deposition of SiO_2 (2 μm in thickness) and subsequent high-temperature (600 °C) annealing in air removes the polymer and converts the PDMS adhesive layer into SiO_2. Melting a powder of AgCl-KCl on top of the cage results in flow of the eutectic along the ribbons of the cage. As the temperature reaches values below the eutectic temperature (~319 °C), periodic lamellar motifs (spacings of ~400 nm) form in guided structures along the ribbons (Fig. 5d–f). This geometrically templated phase separation in 3D space yields unique optical properties due to the periodic variations in refractive index in the structure, suggesting opportunities for optical metamaterials that operate in visible and infrared wavelength regimes.

The compressive buckling approach can yield structures that embed high-performance semiconductor devices, including those that incorporate Si nanomembrane-based electronic devices, such as n- and p-channel MOSFETs (nMOS and pMOS), and diodes into complex 3D layouts [63]. An optical image of an array of nMOS transistors configured in a 3D interconnected bridge structure appears in Fig. 5d. Each device includes 300 nm Si, 100 nm SiO_2, and 5/200 nm Cr/Au layers, with a maximum bending strain of 0.2% strain, which is much lower than the fracture strains of Si (~1%) and SiO_2 (~1.2%) [255–257]. An important point in this context is that size-dependent mechanical properties of materials in the nanoscale regime may lead to buckling mechanics and fracture limits that differ from those of the same materials in bulk forms [258]. For instance, single crystalline silicon nanowires with diameters below 60 nm exhibit significantly increased fracture strength (> 10 GPa) and strain (> 10%) [259,260]; amorphous materials such as SiO_2 nanowires display a brittle-to-ductile transition when the structure diameter is below 18 nm [261]. These and other size related effects may provide additional design opportunities for compressive buckling-based approaches to 3D functional nanostructures.

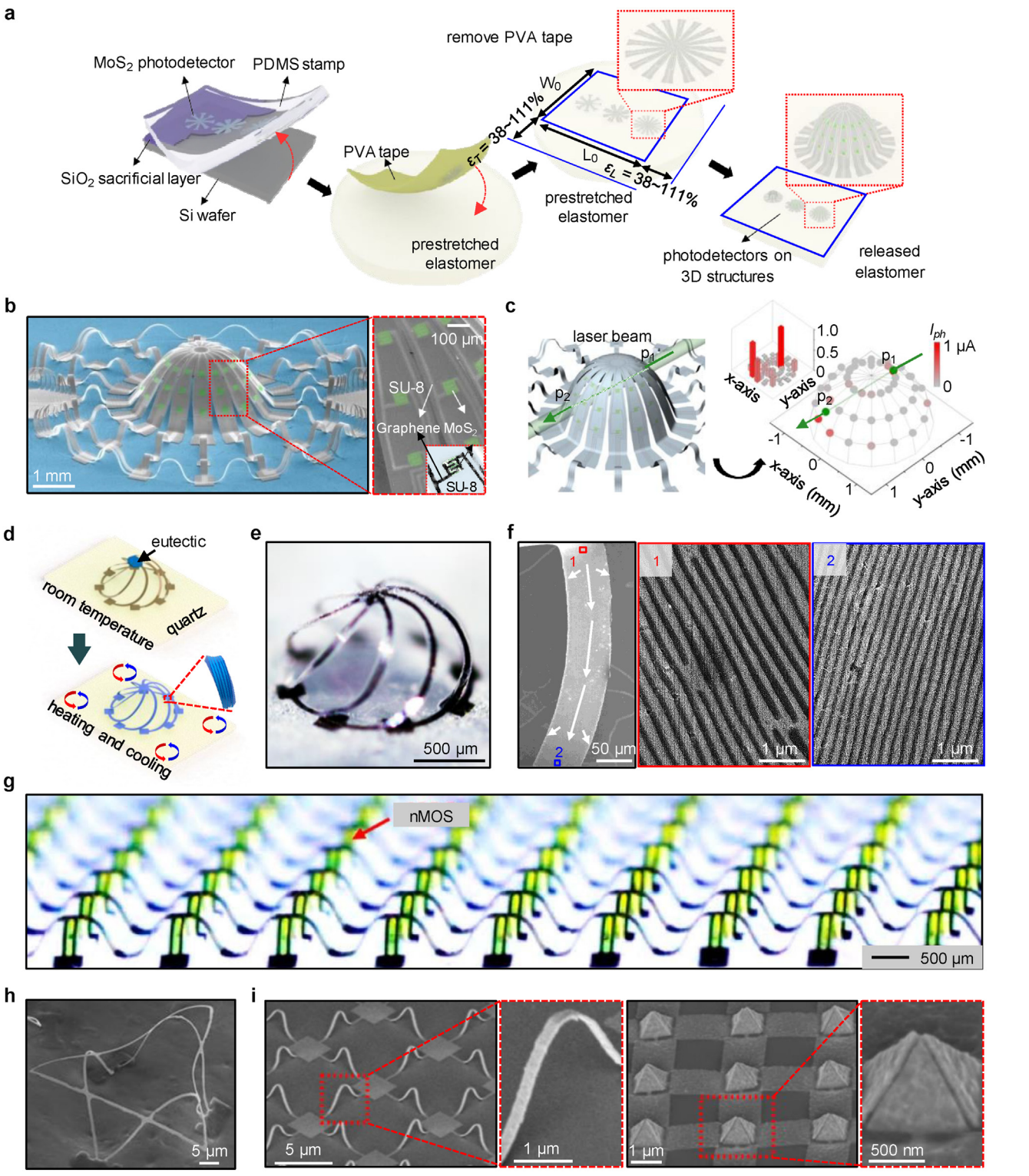

Fig. 5. Guided assembly of functional 3D nanostructures by substrate deformation. a) Scheme illustrating the compressive buckling-induced transformation of a MoS_2/graphene photodetector array from a 2D layout to a 3D hemispherical configuration. b) Colorized SEM images of a 3D hemispherical structure consisting of 48 MoS_2/graphene photodetecting units and interconnects. c) Real-time mapping of the intensity and light direction through 3D photodetector arrays. Panels a–c are adapted from [6]. d) Schematic illustration of the process of guided solidification of AgCl–KCl eutectic on 3D cage structures. e) Optical image of a 3D cage structure of Si-SiO_2 bilayers. f) SEM images of a 3D ribbon covered with solidified AgCl–KCl eutectic material and corresponding high-magnification images at the top and bottom of the ribbon. Panels d–f are adapted from [65]. g) Optical image of a 3D nMOS transistor array based on silicon nanomembrane. Adapted with permission from American Chemical Society [63]. h) SEM image of a 3D silicon ribbon structure at sub-micron scale. Adapted with permission from AAAS [56]. i) SEM images of an array of 3D nanostructures in gold formed by compressive buckling. Adapted with permission from American Chemical Society [262].

Such straightforward 3D shape transformations are compatible with many other materials and device designs. Hence, achieving these 3D structures has direct implications in other areas of technology related to energy storage, photovoltaics, optoelectronics, and many others.

Mechanically guided assembly methods can directly form 3D nanostructures when the 2D precursors are patterned with key dimensions in the submicron regime. One such example is a 3D silicon starfish structure with struts that have widths of 800 nm and thicknesses of 100 nm (Fig. 5h) [56]. More recently, a metal-assisted transfer strategy applied to this compressive buckling process enables formation of 3D gold nanostructures on elastic substrates [262]. The introduction of a silver film between patterned 2D nanostructures and silicon substrates facilitates the transfer onto elastic substrates. By specially designing the 2D precursors to include relatively large areas for improved adhesion to the elastic substrates and narrow, smaller areas for buckling, wide-ranging 3D structures can be achieved in a single-step process, including 3D bridge features and pyramid arrays (Fig. 5i). These mechanically assembled 3D structures can incorporate submicrometer features by use of electron beam lithography methods for forming the 2D precursors. Such types of 3D metallic nanostructures have implications for a variety of applications in nano-optics and optoelectronics.

Conclusions

This review summarizes advances in techniques for fabrication and use of 3D nanoscale architectures in various functional systems. The approaches include top-down techniques for forming nano-sized structures from bulk or thin film materials through lithography and etching processes, bottom-up techniques based on self-assembly of molecules and particles, and assembly approaches that involve 2D to 3D shape transformations driven by internal stress, external forces or substrate deformations with designs inspired by origami and kirigami arts. A variety of materials ranging from high-performance inorganic semiconductors to 2D materials such as graphene and MoS_2, can be incorporated into such 3D nanostructures, where the suitability of the approach depends on the type of material, 3D design, and target function. The resulting 3D systems create interesting and unusual engineering design opportunities in electronics, optoelectronics, photonics, bio-integrated devices and others, as demonstrated by a variety of application examples. Practical implementation of such 3D techniques involves many significant engineering challenges, but success in this endeavor will creates interesting frontiers for next-generation devices with structures and functionalities that cannot be achieved using conventional 2D techniques.

Declaration of Competing Interest

The authors declare that they have no known competing financial interests or personal relationships that could have appeared to influence the work reported in this paper.

Acknowledgements

J.-H. Ahn acknowledges support from the National Research Foundation of Korea (NRF-2015R1A3A2066337).

References

[1] X. Ning, X. Wang, Y. Zhang, X. Yu, D. Choi, N. Zheng, D.S. Kim, Y. Huang, Y. Zhang, J.A. Rogers,Adv. Mater. Interfaces 5 (2018), 1800284.
[2] Y. Ma, X. Feng, J.A. Rogers, Y. Huang, Y. Zhang, Lab Chip 17 (2017) 1689–1704.
[3] Y. Zhang, F. Zhang, Z. Yan, Q. Ma, X. Li, Y. Huang, J.A. Rogers, Nat. Rev. Mater. 2 (2017) 17019.
[4] T.G. Leong, A.M. Zarafshar, D.H. Gracias, Small 6 (2010) 792–806.
[5] G. Huang, Y. Mei,Small 14 (2018), 1703665.
[6] W. Lee, Y. Liu, Y. Lee, B.K. Sharma, S.M. Shinde, S.D. Kim, K. Nan, Z. Yan, M. Han, Y. Huang, Y. Zhang, J.-H. Ahn, J.A. Rogers, Nat. Commun. 9 (2018) 1417.
[7] A. Lamoureux, K. Lee, M. Shlian, S.R. Forrest, M. Shtein, Nat. Commun. 6 (2015) 8092.
[8] R. Feiner, L. Engel, S. Fleischer, M. Malki, I. Gal, A. Shapira, Y. Shacham-Diamand, T. Dvir, Nat. Mater. 15 (2016) 679–685.
[9] P. Froeter, Y. Huang, O.V. Cangellaris, W. Huang, E.W. Dent, M.U. Gillette, J.C. Williams, X. Li, ACS Nano 8 (2014) 11108–11117.
[10] M.S. Mannoor, Z. Jiang, T. James, Y.L. Kong, K.A. Malatesta, W.O. Soboyejo, N. Verma, D.H. Gracias, M.C. McAlpine, Nano Lett. 13 (2013) 2634–2639.
[11] Y. Morikawa, S. Yamagiwa, H. Sawahata, R. Numano, K. Koida, M. Ishida, T. Kawano,Adv. Healthcare Mater. 7 (2018), 1701100.
[12] C.L. Randall, E. Gultepe, D.H. Gracias, Trends Biotechnol. 30 (2012) 138–146.
[13] Z. Liu, H. Du, J. Li, L. Lu, Z.-Y. Li, N.X. Fang, Sci. Adv. 4 (2018) eaat4436.
[14] H. Ning, J.H. Pikul, R. Zhang, X. Li, S. Xu, J. Wang, J.A. Rogers, W.P. King, P.V. Braun, Proc. Natl. Acad. Sci. U. S. A. 112 (2015) 6573–6578.
[15] J.I. Hur, L.C. Smith, B. Dunn, Joule 2 (2018) 1187–1201.
[16] S. Takahashi, K. Suzuki, M. Okano, M. Imada, T. Nakamori, Y. Ota, K. Ishizaki, S. Noda, Nat. Mater. 8 (2009) 721–725.
[17] M.J. Burek, Y. Chu, M.S. Liddy, P. Patel, J. Rochman, S. Meesala, W. Hong, Q. Quan, M.D. Lukin, M. Lončar, Nat. Commun. 5 (2014) 5718.
[18] C. Xu, B.M. Gallant, P.U. Wunderlich, T. Lohmann, J.R. Greer, ACS Nano 9 (2015) 5876–5883.
[19] J.K. Gansel, M. Thiel, M.S. Rill, M. Decker, K. Bade, V. Saile, G. von Freymann, S. Linden, M. Wegener, Science 325 (2009) 1513–1515.
[20] J. Kim, J.A. Hanna, M. Byun, C.D. Santangelo, R.C. Hayward, Science 335 (2012) 1201–1205.
[21] Y.-S. Guan, Z. Zhang, Y. Tang, J. Yin, S. Ren,Adv. Mater. 30 (2018), 1706390.
[22] J. Jiang, S. Zhang, Z. Qian, N. Qin, W. Song, L. Sun, Z. Zhou, Z. Shi, L. Chen, X. Li,Adv. Mater. 30 (2018), 1705919.
[23] T.I. Löbling, J.S. Haataja, C.V. Synatschke, F.H. Schacher, M. Müller, A. Hanisch, A.H. Gröschel, A.H.E. Müller, ACS Nano 8 (2014) 11330–11340.
[24] K. Ma, Y. Gong, T. Aubert, M.Z. Turker, T. Kao, P.C. Doerschuk, U. Wiesner, Nature 558 (2018) 577–580.
[25] X. Liu, F. Zhang, X. Jing, M. Pan, P. Liu, W. Li, B. Zhu, J. Li, H. Chen, L. Wang, J. Lin, Y. Liu, D. Zhao, H. Yan, C. Fan, Nature 559 (2018) 593–598.
[26] A.G. Mark, J.G. Gibbs, T.-C. Lee, P. Fischer, Nat. Mater. 12 (2013) 802–807.
[27] O.G. Schmidt, K. Eberl, Nature 410 (2001) 168.
[28] Z. Tian, L. Zhang, Y. Fang, B. Xu, S. Tang, N. Hu, Z. An, Z. Chen, Y. Mei,Adv. Mater. 29 (2017), 1604572.
[29] J.-H. Cho, M.D. Keung, N. Verellen, L. Lagae, V.V. Moshchalkov, P. Van Dorpe, D.H. Gracias, Small 7 (2011) 1943–1948.
[30] J. Cools, Q. Jin, E. Yoon, D. Alba Burbano, Z. Luo, D. Cuypers, G. Callewaert, D. Braeken, D.H. Gracias,Adv. Sci. 5 (2018), 1700731.
[31] Q. Guo, Z. Di, M.G. Lagally, Y. Mei, Mater. Sci. Eng. R Rep. 128 (2018) 1–31.
[32] Y. Yu, M. Nakano, T. Ikeda, Nature 425 (2003) 145.
[33] K.E. Laflin, C.J. Morris, T. Muqeem, D.H. Gracias,Appl. Phys. Lett. 101 (2012), 131901.
[34] Q. Zhao, W. Zou, Y. Luo, T. Xie,Sci. Adv. 2 (2016), e1501297.
[35] E. Gultepe, J.S. Randhawa, S. Kadam, S. Yamanaka, F.M. Selaru, E.J. Shin, A.N. Kalloo, D.H. Gracias, Adv. Mater. 25 (2013) 514–519.
[36] N. Bassik, B.T. Abebe, K.E. Laflin, D.H. Gracias, Polymer 51 (2010) 6093–6098.
[37] J.S. Randhawa, T.G. Leong, N. Bassik, B.R. Benson, M.T. Jochmans, D.H. Gracias, J. Am. Chem. Soc. 130 (2008) 17238–17239.
[38] A. Sydney Gladman, E.A. Matsumoto, R.G. Nuzzo, L. Mahadevan, J.A. Lewis, Nat. Mater. 15 (2016) 413–418.
[39] Y. Yang, E.M. Terentjev, Y. Wei, Y. Ji, Nat. Commun. 9 (2018) 1906.
[40] L. Huang, R. Jiang, J. Wu, J. Song, H. Bai, B. Li, Q. Zhao, T. Xie,Adv. Mater. 29 (2017), 1605390.
[41] M. Jamal, A.M. Zarafshar, D.H. Gracias, Nat. Commun. 2 (2011) 527.
[42] M. Su, Z. Huang, Y. Li, X. Qian, Z. Li, X. Hu, Q. Pan, F. Li, L. Li, Y. Song,Adv. Mater. 30 (2018), 1703963.
[43] M. Schenk, S.D. Guest, Proc. Natl. Acad. Sci. U. S. A. 110 (2013) 3276–3281.
[44] V.B. Shenoy, D.H. Gracias, MRS Bull. 37 (2012) 847–854.
[45] M.K. Blees, A.W. Barnard, P.A. Rose, S.P. Roberts, K.L. McGill, P.Y. Huang, A.R. Ruyack, J.W. Kevek, B. Kobrin, D.A. Muller, Nature 524 (2015) 204–207.
[46] W.S.Y. Wong, M. Li, D.R. Nisbet, V.S.J. Craig, Z. Wang, A. Tricoli,Sci. Adv. 2 (2016), e1600417.
[47] H. Zhang, X. Yu, P.V. Braun, Nat. Nanotech. 6 (2011) 277–281.
[48] J. Rogers, Y. Huang, O.G. Schmidt, D.H. Gracias, MRS Bull. 41 (2016) 123–129.
[49] Z. Song, T. Ma, R. Tang, Q. Cheng, X. Wang, D. Krishnaraju, R. Panat, C.K. Chan, H. Yu, H. Jiang, Nat. Commun. 5 (2014) 3140.
[50] K. Zhang, Y.H. Jung, S. Mikael, J.-H. Seo, M. Kim, H. Mi, H. Zhou, Z. Xia, W. Zhou, S. Gong, Nat. Commun. 8 (2017) 1782.
[51] P.-K. Yang, Z.-H. Lin, K.C. Pradel, L. Lin, X. Li, X. Wen, J.-H. He, Z.L. Wang, ACS Nano 9 (2015) 901–907.
[52] T. Kim, J.S. Price, A. Grede, S. Lee, G. Choi, W. Guan, T.N. Jackson, N.C. Giebink,Adv. Mater. Technol. 3 (2018), 1800067.
[53] D.-Y. Khang, H. Jiang, Y. Huang, J.A. Rogers, Science 311 (2006) 208–212.
[54] Y. Sun, V. Kumar, I. Adesida, J.A. Rogers, Adv. Mater. 18 (2006) 2857–2862.
[55] S. Yang, K. Khare, P.-C. Lin, Adv. Funct. Mater. 20 (2010) 2550–2564.

[56] S. Xu, Z. Yan, K.-I. Jang, W. Huang, H. Fu, J. Kim, Z. Wei, M. Flavin, J. McCracken, R. Wang, A. Badea, Y. Liu, D. Xiao, G. Zhou, J. Lee, H.U. Chung, H. Cheng, W. Ren, A. Banks, X. Li, U. Paik, R.G. Nuzzo, Y. Huang, Y. Zhang, J.A. Rogers, Science 347 (2015) 154–159.
[57] Y. Zhang, Z. Yan, K. Nan, D. Xiao, Y. Liu, H. Luan, H. Fu, X. Wang, Q. Yang, J. Wang, W. Ren, H. Si, F. Liu, L. Yang, H. Li, J. Wang, X. Guo, H. Luo, L. Wang, Y. Huang, J.A. Rogers, Proc. Natl. Acad. Sci. U. S. A. 112 (2015) 11757–11764.
[58] M. Humood, Y. Shi, M. Han, J. Lefebvre, Z. Yan, M. Pharr, Y. Zhang, Y. Huang, J.A. Rogers, A.A. Polycarpou,Small 14 (2018), 1703852.
[59] X. Ning, H. Wang, X. Yu, J.A.N.T. Soares, Z. Yan, K. Nan, G. Velarde, Y. Xue, R. Sun, Q. Dong, H. Luan, C.M. Lee, A. Chempakasseril, M. Han, Y. Wang, L. Li, Y. Huang, Y. Zhang, J.A. Rogers,Adv. Funct. Mater. 27 (2017), 1605914.
[60] B.H. Kim, F. Liu, Y. Yu, H. Jang, Z. Xie, K. Li, J. Lee, J.Y. Jeong, A. Ryu, Y. Lee, D.H. Kim, X. Wang, K. Lee, J.Y. Lee, S.M. Won, N. Oh, J. Kim, J.Y. Kim, S.-J. Jeong, K.-I. Jang, S. Lee, Y. Huang, Y. Zhang, J.A. Rogers,Adv. Funct. Mater. 28 (2018), 1803149.
[61] K.-I. Jang, K. Li, H.U. Chung, S. Xu, H.N. Jung, Y. Yang, J.W. Kwak, H.H. Jung, J. Song, C. Yang, A. Wang, Z. Liu, J.Y. Lee, B.H. Kim, J.-H. Kim, J. Lee, Y. Yu, B.J. Kim, H. Jang, K.J. Yu, J. Kim, J.W. Lee, J.-W. Jeong, Y.M. Song, Y. Huang, Y. Zhang, J.A. Rogers, Nat. Commun. 8 (2017) 15894.
[62] Z. Yan, T. Pan, G. Yao, F. Liao, Z. Huang, H. Zhang, M. Gao, Y. Zhang, Y. Lin, Sci. Rep. 7 (2017) 42227.
[63] B.H. Kim, J. Lee, S.M. Won, Z. Xie, J.-K. Chang, Y. Yu, Y.K. Cho, H. Jang, J.Y. Jeong, Y. Lee, A. Ryu, D.H. Kim, K.H. Lee, J.Y. Lee, F. Liu, X. Wang, Q. Huo, S. Min, D. Wu, B. Ji, A. Banks, J. Kim, N. Oh, H.M. Jin, S. Han, D. Kang, C.H. Lee, Y.M. Song, Y. Zhang, Y. Huang, K.-I. Jang, J.A. Rogers, ACS Nano 12 (2018) 4164–4171.
[64] K.P. Dhakal, S. Roy, H. Jang, X. Chen, W.S. Yun, H. Kim, J. Lee, J. Kim, J.-H. Ahn, Chem. Mater. 29 (2017) 5124–5133.
[65] Z. Yan, M. Han, Y. Shi, A. Badea, Y. Yang, A. Kulkarni, E. Hanson, M.E. Kandel, X. Wen, F. Zhang, Y. Luo, Q. Lin, H. Zhang, X. Guo, Y. Huang, K. Nan, S. Jia, A.W. Oraham, M.B. Mevis, J. Lim, X. Guo, M. Gao, W. Ryu, K.J. Yu, B.G. Nicolau, A. Petronico, S.S. Rubakhin, J. Lou, P.M. Ajayan, K. Thornton, G. Popescu, D. Fang, J.V. Sweedler, P.V. Braun, H. Zhang, R.G. Nuzzo, Y. Huang, Y. Zhang, J.A. Rogers, Proc. Natl. Acad. Sci. U. S. A. 114 (2017) E9455–E9464.
[66] J.M. McCracken, S. Xu, A. Badea, K.-I. Jang, Z. Yan, D.J. Wetzel, K. Nan, Q. Lin, M. Han, M.A. Anderson, J.W. Lee, Z. Wei, M. Pharr, R. Wang, J. Su, S.S. Rubakhin, J.V. Sweedler, J.A. Rogers, R.G. Nuzzo,Adv. Biosyst. 1 (2017), 1700068.
[67] X. Ning, X. Yu, H. Wang, R. Sun, R.E. Corman, H. Li, C.M. Lee, Y. Xue, A. Chempakasseril, Y. Yao, Z. Zhang, H. Luan, Z. Wang, W. Xia, X. Feng, R.H. Ewoldt, Y. Huang, Y. Zhang, J.A. Rogers, Sci. Adv. 4 (2018) eaat8313.
[68] K. Nan, H. Luan, Z. Yan, X. Ning, Y. Wang, A. Wang, J. Wang, M. Han, M. Chang, K. Li, Y. Zhang, W. Huang, Y. Xue, Y. Huang, Y. Zhang, J.A. Rogers,Adv. Funct. Mater. 27 (2017), 1604281.
[69] Y. Tan, Z. Chu, Z. Jiang, T. Hu, G. Li, J. Song, ACS Nano 11 (2017) 6843–6852.
[70] M. Aoki, J.-Y. Juang,Royal Soc. Open Sci. 5 (2018), 171962.
[71] M.A. Yoder, Z. Yan, M. Han, J.A. Rogers, R.G. Nuzzo, J. Am. Chem. Soc. 140 (2018) 9001–9019.
[72] H.C. Ko, A.J. Baca, J.A. Rogers, Nano Lett. 6 (2006) 2318–2324.
[73] M. Hentschel, M. Schäferling, X. Duan, H. Giessen, N. Liu,Sci. Adv. 3 (2017), e1602735.
[74] G. von Freymann, A. Ledermann, M. Thiel, I. Staude, S. Essig, K. Busch, M. Wegener, Adv. Funct. Mater. 20 (2010) 1038–1052.
[75] T. Ergin, N. Stenger, P. Brenner, J.B. Pendry, M. Wegener, Science 328 (2010) 337–339.
[76] J.S. Randhawa, K.E. Laflin, N. Seelam, D.H. Gracias, Adv. Funct. Mater. 21 (2011) 2395–2410.
[77] A. Marino, J. Barsotti, G. de Vito, C. Filippeschi, B. Mazzolai, V. Piazza, M. Labardi, V. Mattoli, G. Ciofani, ACS Appl. Mater. Interfaces 7 (2015) 25574–25579.
[78] X.H. Qin, X. Wang, M. Rottmar, B.J. Nelson, K.J.A.M. Maniura-Weber,Adv. Mater. 30 (2018), 1705564.
[79] C. Peters, M. Hoop, S. Pané, B.J. Nelson, C.J.A.M. Hierold, Adv. Mater. 28 (2016) 533–538.
[80] L.R. Meza, A.J. Zelhofer, N. Clarke, A.J. Mateos, D.M. Kochmann, J.R. Greer, Proc. Natl. Acad. Sci. U. S. A. 112 (2015) 11502–11507.
[81] M.S. Rill, C. Plet, M. Thiel, I. Staude, G. Von Freymann, S. Linden, M. Wegener, Nat. Mater. 7 (2008) 543–546.
[82] G. Yoon, I. Kim, S. So, J. Mun, M. Kim, J. Rho, Sci. Rep. 7 (2017) 6668.
[83] A. Vyatskikh, S. Delalande, A. Kudo, X. Zhang, C.M. Portela, J.R. Greer, Nat. Commun. 9 (2018) 593.
[84] W. Wu, M. Hu, F.S. Ou, Z. Li, R.S. Williams,Nanotechnology 21 (2010), 255502.
[85] S. Jeon, J.-U. Park, R. Cirelli, S. Yang, C.E. Heitzman, P.V. Braun, P.J. Kenis, J.A. Rogers, Proc. Natl. Acad. Sci. U. S. A. 101 (2004) 12428–12433.
[86] X. Xu, Q. Yang, N. Wattanatorn, C. Zhao, N. Chiang, S.J. Jonas, P.S. Weiss, ACS Nano 11 (2017) 10384–10391.
[87] L. Wen, R. Xu, Y. Mi, Y. Lei, Nat. Nanotech. 12 (2017) 244–250.
[88] X. Zheng, H. Lee, T.H. Weisgraber, M. Shusteff, J. DeOtte, E.B. Duoss, J.D. Kuntz, M.M. Biener, Q. Ge, J.A. Jackson, Science 344 (2014) 1373–1377.
[89] F. Yesilkoy, V. Flauraud, M. Rüegg, B. Kim, J. Brugger, Nanoscale 8 (2016) 4945–4950.
[90] Y.J.M.E. Chen, Microelectron. Eng. 135 (2015) 57–72.
[91] A.A. Tseng, K. Chen, C.D. Chen, K.J. Ma, IEEE Trans. Electron. Packag. Manuf. 26 (2003) 141–149.
[92] S. Maruo, J.T. Fourkas, Laser Photonics Rev. 2 (2008) 100–111.
[93] L. Li, J.T. Fourkas, Mater. Today 10 (2007) 30–37.
[94] C.N. LaFratta, J.T. Fourkas, T. Baldacchini, R.A. Farrer, Angew. Chem. Int. Ed. 46 (2007) 6238–6258.
[95] M.C. Traub, W. Longsine, V.N. Truskett, Annu. Rev. Chem. Biomol. Eng. 7 (2016) 583–604.
[96] H. Schift, J. Vac. Sci. Technol. B 26 (2008) 458–480.
[97] J.H. Jang, C.K. Ullal, M. Maldovan, T. Gorishnyy, S. Kooi, C. Koh, E.L. Thomas, Adv. Funct. Mater. 17 (2007) 3027–3041.
[98] H.-D. Yu, M.D. Regulacio, E. Ye, M.-Y. Han, Chem. Soc. Rev. 42 (2013) 6006–6018.
[99] D. Xia, Z. Ku, S. Lee, S. Brueck, Adv. Mater. 23 (2011) 147–179.
[100] I. Wathuthanthri, Y. Liu, K. Du, W. Xu, C.H. Choi, Adv. Funct. Mater. 23 (2013) 608–618.
[101] T. Jeon, D.-H. Kim, S.-G. Park,Adv. Mater. Interfaces 5 (2018), 1800330.
[102] D.C. Meisel, M. Wegener, K. Busch,Phys. Rev. B 70 (2004), 165104.
[103] H.H. Solak, D. He, W. Li, S. Singh-Gasson, F. Cerrina, B.-H. Sohn, X. Yang, P. Nealey, Appl. Phys. Lett. 75 (1999) 2328–2330.
[104] J. Billaud, F. Bouville, T. Magrini, C. Villevieille, A.R. Studart, Nat. Energy 1 (2016) 16097.
[105] Y. Liu, D. Lin, Z. Liang, J. Zhao, K. Yan, Y. Cui, Nat. Commun. 7 (2016) 10992.
[106] L. Yuan, P.R. Herman, Sci. Rep. 6 (2016) 22294.
[107] S.-G. Park, S.-K. Lee, J.H. Moon, S.-M. Yang, Lab Chip 9 (2009) 3144–3150.
[108] Y. Zhou, X.Y. Chen, Y.H. Fu, G. Vienne, A.I. Kuznetsov, B. Luk'yanchuk,Appl. Phys. Lett. 103 (2013), 123116.
[109] M.C. George, E.C. Nelson, J.A. Rogers, P.V. Braun, Angew. Chem. Int. Ed. 48 (2009) 144–148.
[110] J. Park, J.H. Park, E. Kim, C.W. Ahn, H.I. Jang, J.A. Rogers, S. Jeon, Adv. Mater. 23 (2011) 860–864.
[111] D.J. Shir, S. Jeon, H. Liao, M. Highland, D.G. Cahill, M.F. Su, I.F. El-Kady, C.G. Christodoulou, G.R. Bogart, A.V. Hamza, J.A. Rogers, J. Phys. Chem. B 111 (2007) 12945–12958.
[112] C.H. Chang, L. Tian, W.R. Hesse, H. Gao, H.J. Choi, J.G. Kim, M. Siddiqui, G. Barbastathis, Nano Lett. 11 (2011) 2533–2537.
[113] J.-H. Min, X.A. Zhang, C.-H. Chang, Opt. Express 24 (2016) A276–A284.
[114] X.A. Zhang, J. Elek, C.-H. Chang, ACS Nano 7 (2013) 6212–6218.
[115] Y.W. Kwon, J. Park, T. Kim, S.H. Kang, H. Kim, J. Shin, S. Jeon, S.W. Hong, ACS Nano 10 (2016) 4609–4617.
[116] T.Y. Jeon, J.H. Kim, S.-G. Park, J.-D. Kwon, D.-H. Kim, S.-H. Kim, Adv. Opt. Mater. 4 (2016) 1893–1900.
[117] J. Park, S. Wang, M. Li, C. Ahn, J.K. Hyun, D.S. Kim, D.K. Kim, J.A. Rogers, Y. Huang, S. Jeon, Nat. Commun. 3 (2012) 916.
[118] J. Park, J. Seo, H.K. Jung, G. Hyun, S.Y. Park, S. Jeon, Adv. Funct. Mater. 26 (2016) 7170–7177.
[119] J. Park, K.-I. Kim, K. Kim, D.-C. Kim, D. Cho, J.H. Lee, S. Jeon, Adv. Mater. 27 (2015) 8000–8006.
[120] X.A. Zhang, A. Bagal, E.C. Dandley, J. Zhao, C.J. Oldham, B.-I. Wu, G.N. Parsons, C.-H. Chang, Adv. Funct. Mater. 25 (2015) 6644–6649.
[121] C. Ahn, S.-M. Kim, J.-W. Jung, J. Park, T. Kim, S.E. Lee, D. Jang, J.-W. Hong, S.M. Han, S. Jeon, ACS Nano 12 (2018) 9126–9133.
[122] S.-W. Lee, M. Jafary-Zadeh, D.Z. Chen, Y.-W. Zhang, J.R. Greer, Nano Lett. 15 (2015) 5673–5681.
[123] J. Chen, Y. Zhou, D. Wang, F. He, V.M. Rotello, K.R. Carter, J.J. Watkins, S.R. Nugen, Lab Chip 15 (2015) 3086–3094.
[124] M. Karl, J.M. Glackin, M. Schubert, N.M. Kronenberg, G.A. Turnbull, I.D. Samuel, M.C. Gather, Nat. Commun. 9 (2018) 1525.
[125] D. Franklin, Y. Chen, A. Vazquez-Guardado, S. Modak, J. Boroumand, D. Xu, S.-T. Wu, D. Chanda, Nat. Commun. 6 (2015) 7337.
[126] M.W. Knight, L. Liu, Y. Wang, L. Brown, S. Mukherjee, N.S. King, H.O. Everitt, P. Nordlander, N.J. Halas, Nano Lett. 12 (2012) 6000–6004.
[127] M.W. Knight, N.S. King, L. Liu, H.O. Everitt, P. Nordlander, N.J. Halas, ACS Nano 8 (2013) 834–840.
[128] T. Xu, Y.-K. Wu, X. Luo, L.J. Guo, Nat. Commun. 1 (2010) 59.
[129] K. Aydin, V.E. Ferry, R.M. Briggs, H.A. Atwater, Nat. Commun. 2 (2011) 517.
[130] J. Olson, A. Manjavacas, L. Liu, W.-S. Chang, B. Foerster, N.S. King, M.W. Knight, P. Nordlander, N.J. Halas, S. Link, Proc. Natl. Acad. Sci. U. S. A. 111 (2014) 14348–14353.
[131] X.M. Goh, Y. Zheng, S.J. Tan, L. Zhang, K. Kumar, C.-W. Qiu, J.K. Yang, Nat. Commun. 5 (2014) 5361.
[132] W. Zhang, L.-H. Han, S. Chen,J. Manuf. Sci. Eng. 132 (2010), 030907.
[133] N. Chidambaram, R. Kirchner, M. Altana, H. Schift,J. Vac. Sci. Technol. B 34 (2016), 06K401.
[134] Q. Hu, X.-Z. Sun, C.D. Parmenter, M.W. Fay, E.F. Smith, G.A. Rance, Y. He, F. Zhang, Y. Liu, D. Irvine, Sci. Rep. 7 (2017) 17150.
[135] D.W. Yee, M.L. Lifson, B.W. Edwards, J.R. Greer,Adv. Mater. (2019), 1901345.
[136] S. Wong, M. Deubel, F. Pérez-Willard, S. John, G.A. Ozin, M. Wegener, G. von Freymann, Adv. Mater. 18 (2006) 265–269.
[137] Y. Chen, K. Bi, Q. Wang, M. Zheng, Q. Liu, Y. Han, J. Yang, S. Chang, G. Zhang, H. Duan, ACS Nano 10 (2016) 11228–11236.
[138] S.C. Lee, A. Neumann, Y.B. Jiang, K. Artyushkova, S.R.J. Brueck,Nanotechnology 27 (2016), 375707.
[139] S.C. Warren-Smith, R.M. André, C. Perrella, J. Dellith, H. Bartelt, Opt. Express 24 (2016) 378–387.
[140] K. Grandfield, H. Engqvist,Adv. Mater. Sci. Eng. 2012 (2012), 841961.
[141] M.V. Gorkunov, V.E. Dmitrienko, A.A. Ezhov, V.V. Artemov, O.Y. Rogov, Sci. Rep. 5 (2015) 9273.

[142] M.V. Gorkunov, A.A. Ezhov, V.V. Artemov, O.Y. Rogov, S.G. Yudin,Appl. Phys. Lett. 104 (2014), 221102.
[143] O.Y. Rogov, V.V. Artemov, M.V. Gorkunov, A.A. Ezhov, D.N. Khmelenin, J. Microsc. 268 (2017) 254–258.
[144] M.J. Burek, N.P. de Leon, B.J. Shields, B.J. Hausmann, Y. Chu, Q. Quan, A.S. Zibrov, H. Park, M.D. Lukin, M. Lončar, Nano Lett. 12 (2012) 6084–6089.
[145] K. Suzuki, K. Kitano, K. Ishizaki, S. Noda, Opt. Express 22 (2014) 17099–17106.
[146] O.J. Hildreth, A.G. Fedorov, C.P. Wong, ACS Nano 6 (2012) 10004–10012.
[147] K. Yamada, M. Yamada, H. Maki, K. Itoh,Nanotechnology 29 (2018), 28LT01.
[148] A. Reisman, M. Berkenblit, S.A. Chan, F.B. Kaufman, D.C. Green, J. Electrochem. Soc. 126 (1979) 1406–1415.
[149] K. Shimizu, S. Oda, M. Matsumura, Jpn. J. Appl. Phys. 27 (1988) L1778.
[150] H. Seidel, L. Csepregi, A. Heuberger, H. Baumgärtel, J. Electrochem. Soc. 137 (1990) 3626–3632.
[151] P. Sievilä, N. Chekurov, I. Tittonen,Nanotechnology 21 (2010), 145301.
[152] G.T.A. Kovacs, N.I. Maluf, K.E. Petersen, Proc. IEEE 86 (1998) 1536–1551.
[153] K.R. Williams, R.S. Muller, J. Microelectromech. Syst. 5 (1996) 256–269.
[154] K.R. Williams, K. Gupta, M. Wasilik, J. Microelectromech. Syst. 12 (2003) 761–778.
[155] B. Salhi, D. Troadec, R. Boukherroub,Nanotechnology 28 (2017), 205301.
[156] N. Chekurov, K. Grigoras, A. Peltonen, S. Franssila, I. Tittonen,Nanotechnology 20 (2009), 065307.
[157] Z. Han, E. Salmi, M. Vehkamäki, M. Leskelä, M. Ritala,Nanotechnology 29 (2018), 055301.
[158] C.N. Kaplan, W.L. Noorduin, L. Li, R. Sadza, L. Folkertsma, J. Aizenberg, L. Mahadevan, Science 355 (2017) 1395–1399.
[159] P. De Coppi, G. Bartsch Jr, M.M. Siddiqui, T. Xu, C.C. Santos, L. Perin, G. Mostoslavsky, A.C. Serre, E.Y. Snyder, J.J. Yoo, M.E. Furth, S. Soker, A. Atala, Nat. Biotechnol. 25 (2007) 100–106.
[160] D. Han, X. Qi, C. Myhrvold, B. Wang, M. Dai, S. Jiang, M. Bates, Y. Liu, B. An, F. Zhang, H. Yan, P. Yin, Science 358 (2017) eaao2648.
[161] K. Miszta, J. De Graaf, G. Bertoni, D. Dorfs, R. Brescia, S. Marras, L. Ceseracciu, R. Cingolani, R. Van Roij, M. Dijkstra, Nat. Mater. 10 (2011) 872–876.
[162] A. Nych, U. Ognysta, M. Škarabot, M. Ravnik, S. Žumer, I. Muševič, Nat. Commun. 4 (2013) 1489.
[163] F. Hong, F. Zhang, Y. Liu, H. Yan, Chem. Rev. 117 (2017) 12584–12640.
[164] C.A. Ross, K.K. Berggren, J.Y. Cheng, Y.S. Jung, J.B. Chang, Adv. Mater. 26 (2014) 4386–4396.
[165] S.H. Yoo, H.-S. Lee, Acc. Chem. Res. 50 (2017) 832–841.
[166] D.A. Pawlak, S. Turczynski, M. Gajc, K. Kolodziejak, R. Diduszko, K. Rozniatowski, J. Smalc, I. Vendik, Adv. Funct. Mater. 20 (2010) 1116–1124.
[167] H. Qiu, Z.M. Hudson, M.A. Winnik, I. Manners, Science 347 (2015) 1329–1332.
[168] A. Hanisch, A.H. Gröschel, M. Förtsch, M. Drechsler, H. Jinnai, T.M. Ruhland, F.H. Schacher, A.H.E. Müller, ACS Nano 7 (2013) 4030–4041.
[169] F.S. Bates, G.H. Fredrickson, Phys. Today 52 (2000) 32–38.
[170] V. Castelletto, I.W. Hamley, Curr. Opin. Solid State Mater. Sci. 8 (2004) 426–438.
[171] C. Guo, Y.-H. Lin, M.D. Witman, K.A. Smith, C. Wang, A. Hexemer, J. Strzalka, E.D. Gomez, R. Verduzco, Nano Lett. 13 (2013) 2957–2963.
[172] Y. Kambe, C.G. Arges, S. Patel, M.P. Stoykovish, P.F. Nealey, Electrochem. Soc. Interface 26 (2017) 61–67.
[173] R. Dehmel, A. Nicolas, M.R. Scherer, U. Steiner, Adv. Funct. Mater. 25 (2015) 6900–6905.
[174] J.A. Dolan, B.D. Wilts, S. Vignolini, J.J. Baumberg, U. Steiner, T.D. Wilkinson, Adv. Opt. Mater. 3 (2015) 12–32.
[175] S. Salvatore, S. Vignolini, J. Philpott, M. Stefik, U. Wiesner, J.J. Baumberg, U. Steiner, Nanoscale 7 (2015) 1032–1036.
[176] S.Z. Bas, C. Cummins, D. Borah, M. Ozmen, M.A. Morris, Anal. Chem. 90 (2017) 1122–1128.
[177] P. Mokarian-Tabari, R. Senthamaraikannan, C. Glynn, T.W. Collins, C. Cummins, D. Nugent, C. O'Dwyer, M.A. Morris, Nano Lett. 17 (2017) 2973–2978.
[178] A. Cangialosi, C. Yoon, J. Liu, Q. Huang, J. Guo, T.D. Nguyen, D.H. Gracias, R. Schulman, Science 357 (2017) 1126–1130.
[179] A. Kuzyk, R. Schreiber, Z. Fan, G. Pardatscher, E.-M. Roller, A. Högele, F.C. Simmel, A.O. Govorov, T. Liedl, Nature 483 (2012) 311–314.
[180] D. Han, S. Pal, J. Nangreave, Z. Deng, Y. Liu, H. Yan, Science 332 (2011) 342–346.
[181] H. Dietz, S.M. Douglas, W.M. Shih, Science 325 (2009) 725–730.
[182] P. Wang, T.A. Meyer, V. Pan, P.K. Dutta, Y. Ke, Chem 2 (2017) 359–382.
[183] N.C. Seeman, H.F. Sleiman, Nat. Rev. Mater. 3 (2017) 17068.
[184] W. Stöber, A. Fink, E. Bohn, J. Colloid Interface Sci. 26 (1968) 62–69.
[185] C. Jin, H. Qiu, L. Han, M. Shu, S. Che, Chem. Commun. (2009) 3407–3409.
[186] Y. Ke, L.L. Ong, W.M. Shih, P. Yin, Science 338 (2012) 1177–1183.
[187] L.L. Ong, N. Hanikel, O.K. Yaghi, C. Grun, M.T. Strauss, P. Bron, J. Lai-Kee-Him, F. Schueder, B. Wang, P. Wang, J.Y. Kishi, C. Myhrvold, A. Zhu, R. Jungmann, G. Bellot, Y. Ke, P. Yin, Nature 552 (2017) 72–77.
[188] M. De Volder, S. Park, S. Tawfick, A.J. Hart, Nat. Commun. 5 (2014).
[189] S.J. Park, H. Zhao, S. Kim, M. De Volder, A.J. Hart, Small 12 (2016) 4393–4403.
[190] H. Zhao, S.J. Park, B.R. Solomon, S. Kim, D. Soto, A.T. Paxson, K.K. Varanasi, A.J. Hart,Adv. Mater. 31 (2019), 1807686.
[191] M. Matuschek, D.P. Singh, H.-H. Jeong, M. Nesterov, T. Weiss, P. Fischer, F. Neubrech, N. Liu,Small 14 (2018), 1702990.
[192] K. Robbie, M.J. Brett, A. Lakhtakia, Nature 384 (1996), 616-616.
[193] S. Liedtke, C. Grüner, A. Lotnyk, B. Rauschenbach,Nanotechnology 28 (2017), 385604.
[194] P.C.P. Hrudey, K.L. Westra, M.J. Brett, Adv. Mater. 18 (2006) 224–228.
[195] Y. Luo, C. Chi, M. Jiang, R. Li, S. Zu, Y. Li, Z. Fang,Adv. Opt. Mater. 5 (2017), 1700040.
[196] A. Passaseo, M. Esposito, M. Cuscunà, V. Tasco,Adv. Opt. Mater. 5 (2017), 1601079.
[197] J. Bauer, A. Schroer, R. Schwaiger, O. Kraft, Nat. Mater. 15 (2016) 438–443.
[198] D. Oran, S.G. Rodriques, R. Gao, S. Asano, M.A. Skylar-Scott, F. Chen, P.W. Tillberg, A.H. Marblestone, E.S. Boyden, Science 362 (2018) 1281–1285.
[199] Z. Song, C. Lv, M. Liang, V. Sanphuang, K. Wu, B. Chen, Z. Zhao, J. Bai, X. Wang, J.L. Volakis, L. Wang, X. He, Y. Yao, S. Tongay, H. Jiang, Small 12 (2016) 5401–5406.
[200] W. Xi, C.K. Schmidt, S. Sanchez, D.H. Gracias, R.E. Carazo-Salas, S.P. Jackson, O.G. Schmidt, Nano Lett. 14 (2014) 4197–4204.
[201] Y. Mei, G. Huang, A.A. Solovev, E.B. Ureña, I. Mönch, F. Ding, T. Reindl, R.K.Y. Fu, P.K. Chu, O.G. Schmidt, Adv. Mater. 20 (2008) 4085–4090.
[202] K. Aoki, K. Ishiguro, M. Denokami, Y. Tanahashi, K. Furusawa, N. Sekine, T. Adschiri, M. Fujii,Small 13 (2017), 1701630.
[203] E. Chason, P.R. Guduru,J. Appl. Phys. 119 (2016), 191101.
[204] A.M. Engwall, Z. Rao, E. Chason, Mater. Des. 110 (2016) 616–623.
[205] V. Magdanz, M. Guix, O.G. Schmidt, Robot. Biomim. 1 (2014) 11.
[206] X. Wang, Y. Chen, O.G. Schmidt, C. Yan, Chem. Soc. Rev. 45 (2016) 1308–1330.
[207] H. Wang, H. Zhen, S. Li, Y. Jing, G. Huang, Y. Mei, W. Lu,Sci. Adv. 2 (2016), e1600027.
[208] S. Böttner, M.R. Jorgensen, O.G. Schmidt, Scr. Mater. 122 (2016) 119–124.
[209] X. Liu, T. Ma, Y. Xu, L. Sun, L. Zheng, O.G. Schmidt, J. Zhang, Sens. Actuator B-Chem. 264 (2018) 92–99.
[210] W. Huang, J. Zhou, P.J. Froeter, K. Walsh, S. Liu, M.D. Kraman, M. Li, J.A. Michaels, D.J. Sievers, S. Gong, X. Li, Nat. Electron. 1 (2018) 305–313.
[211] C. Xu, X. Wu, G. Huang, Y. Mei,Adv. Mater. Technol. 4 (2019), 1800486.
[212] V.Y. Prinz, V.A. Seleznev, A.K. Gutakovsky, A.V. Chehovskiy, V.V. Preobrazhenskii, M.A. Putyato, T.A. Gavrilova, Physica E. 6 (2000) 828–831.
[213] G. Mao, Q. Wang, Z. Chai, H. Liu, K. Liu, X. Ren, RSC Adv. 7 (2017) 14481–14486.
[214] Y. Mei, D.J. Thurmer, C. Deneke, S. Kiravittaya, Y.-F. Chen, A. Dadgar, F. Bertram, B. Bastek, A. Krost, J. Christen, T. Reindl, M. Stoffel, E. Coric, O.G. Schmidt, ACS Nano 3 (2009) 1663–1668.
[215] X. Wu, Z. Tian, H. Cong, Y. Wang, R. Edy, G. Huang, Z. Di, C. Xue, Y. Mei,Nanotechnology 29 (2018), 42LT02.
[216] C. Chen, P. Song, F. Meng, X. Li, X. Liu, J. Song,Nanotechnology 28 (2017), 485302.
[217] T.-H. Chang, K. Xiong, S.H. Park, G. Yuan, Z. Ma, J. Han, Sci. Rep. 7 (2017) 6360.
[218] V.Y. Prinz, E.V. Naumova, S.V. Golod, V.A. Seleznev, A.A. Bocharov, V.V. Kubarev, Sci. Rep. 7 (2017) 43334.
[219] M.F. Doerner, W.D. Nix, Crit. Rev. Solid State Mater. Sci. 14 (1988) 225–268.
[220] A. Moridi, H. Ruan, L.C. Zhang, M. Liu, Int. J. Solids Struc. 50 (2013) 3562–3569.
[221] X. Cui, Z. Kong, E. Gao, D. Huang, Y. Hao, H. Shen, C.-a. Di, Z. Xu, J. Zheng, D. Zhu, Nat. Commun. 9 (2018) 1301.
[222] Y. Mao, Y. Zheng, C. Li, L. Guo, Y. Pan, R. Zhu, J. Xu, W. Zhang, W. Wu,Adv. Mater. 29 (2017), 1606482.
[223] J. Li, Z.J.N. Liu, Nanophotonics 7 (2018) 1637–1650.
[224] K. Chalapat, N. Chekurov, H. Jiang, J. Li, B. Parviz, G.S. Paraoanu, Adv. Mater. 25 (2013) 91–95.
[225] Y. Mao, Y. Pan, W. Zhang, R. Zhu, J. Xu, W.J.Nl. Wu, Nano Lett. 16 (2016) 7025–7029.
[226] Z. Liu, S. Du, A. Cui, Z. Li, Y. Fan, S. Chen, W. Li, J. Li, C. Gu,Adv. Mater. 29 (2017), 1606298.
[227] Y. Hu, Z. Lao, B.P. Cumming, D. Wu, J. Li, H. Liang, J. Chu, W. Huang, M. Gu, Proc. Natl. Acad. Sci. U. S. A. 112 (2015) 6876–6881.
[228] W. Li, L. Zhang, X. Ge, B. Xu, W. Zhang, L. Qu, C.-H. Choi, J. Xu, A. Zhang, H. Lee, D.A. Weitz, Chem. Soc. Rev. 47 (2018) 5646–5683.
[229] M. Hu, F.S. Ou, W. Wu, I. Naumov, X. Li, A.M. Bratkovsky, R.S. Williams, Z. Li, J. Am. Chem. Soc. 132 (2010) 12820–12822.
[230] M. De Volder, A.J. Hart, Angew. Chem. Int. Ed. 52 (2013) 2412–2425.
[231] D. Joung, A. Nemilentsau, K. Agarwal, C. Dai, C. Liu, Q. Su, J. Li, T. Low, S.J. Koester, J.-H. Cho, Nano Lett. 17 (2017) 1987–1994.
[232] C. Dai, K. Agarwal, J.-H. Cho, ACS Nano 12 (2018) 10251–10261.
[233] C. Dai, J.-H. Cho, Nano Lett. 16 (2016) 3655–3660.
[234] W. Xu, Z. Qin, C.-T. Chen, H.R. Kwag, Q. Ma, A. Sarkar, M.J. Buehler, D.H. Gracias,Sci. Adv. 3 (2017), e1701084.
[235] Q. Jin, M. Li, B. Polat, S.K. Paidi, A. Dai, A. Zhang, J.V. Pagaduan, I. Barman, D.H. Gracias, Angew. Chem. Int. Ed. 56 (2017) 3822–3826.
[236] M.Z. Miskin, K.J. Dorsey, B. Bircan, Y. Han, D.A. Muller, P.L. McEuen, I. Cohen, Proc. Natl. Acad. Sci. U. S. A. 115 (2018) 466–470.
[237] W.M. Choi, J. Song, D.-Y. Khang, H. Jiang, Y.Y. Huang, J.A. Rogers, Nano Lett. 7 (2007) 1655–1663.
[238] H. Fu, K. Nan, P. Froeter, W. Huang, Y. Liu, Y. Wang, J. Wang, Z. Yan, H. Luan, X. Guo, Y. Zhang, C. Jiang, L. Li, A.C. Dunn, X. Li, Y. Huang, Y. Zhang, J.A. Rogers,Small 13 (2017), 1700151.
[239] Y. Liu, Z. Yan, Q. Lin, X. Guo, M. Han, K. Nan, K.-C. Hwang, Y. Huang, Y. Zhang, J.A. Rogers, Adv. Funct. Mater. 26 (2016) 2909–2918.
[240] Y. Shi, P. Pei, X. Cheng, Z. Yan, M. Han, Z. Li, C. Gao, J.A. Rogers, Y. Huang, Y. Zhang, Soft Matter 14 (2018) 8828–8837.

[241] X. Wang, X. Guo, J. Ye, N. Zheng, P. Kohli, D. Choi, Y. Zhang, Z. Xie, Q. Zhang, H. Luan, K. Nan, B.H. Kim, Y. Xu, X. Shan, W. Bai, R. Sun, Z. Wang, H. Jang, F. Zhang, Y. Ma, Z. Xu, X. Feng, T. Xie, Y. Huang, Y. Zhang, J.A. Rogers,Adv. Mater. 31 (2019), 1805615.
[242] K. Nan, S.D. Kang, K. Li, K.J. Yu, F. Zhu, J. Wang, A.C. Dunn, C. Zhou, Z. Xie, M.T. Agne, H. Wang, H. Luan, Y. Zhang, Y. Huang, G.J. Snyder, J.A. Rogers, Sci. Adv. 4 (2018) eaau5849.
[243] M. Han, H. Wang, Y. Yang, C. Liang, W. Bai, Z. Yan, H. Li, Y. Xue, X. Wang, B. Akar, H. Zhao, H. Luan, J. Lim, I. Kandela, G.A. Ameer, Y. Zhang, Y. Huang, J.A. Rogers, Nat. Electron. 2 (2019) 26–35.
[244] Z. Yan, M. Han, Y. Yang, K. Nan, H. Luan, Y. Luo, Y. Zhang, Y. Huang, J.A. Rogers, Extreme Mech. Lett. 11 (2017) 96–104.
[245] Z. Yan, F. Zhang, J. Wang, F. Liu, X. Guo, K. Nan, Q. Lin, M. Gao, D. Xiao, Y. Shi, Y. Qiu, H. Luan, J.H. Kim, Y. Wang, H. Luo, M. Han, Y. Huang, Y. Zhang, J.A. Rogers, Adv. Funct. Mater. 26 (2017) 2629–2639.
[246] Z. Yan, F. Zhang, F. Liu, M. Han, D. Ou, Y. Liu, Q. Lin, X. Guo, H. Fu, Z. Xie, M. Gao, Y. Huang, J. Kim, Y. Qiu, K. Nan, J. Kim, P. Gutruf, H. Luo, A. Zhao, K.-C. Hwang, Y. Huang, Y. Zhang, J.A. Rogers,Sci. Adv. 2 (2016), e1601014.
[247] H. Fu, K. Nan, W. Bai, W. Huang, K. Bai, L. Lu, C. Zhou, Y. Liu, F. Liu, J. Wang, M. Han, Z. Yan, H. Luan, Y. Zhang, Y. Zhang, J. Zhao, X. Cheng, M. Li, J.W. Lee, Y. Liu, D. Fang, X. Li, Y. Huang, Y. Zhang, J.A. Rogers, Nat. Mater. 17 (2018) 268–276.
[248] H. Zhao, K. Li, M. Han, F. Zhu, A. Vázquez-Guardado, P. Guo, Z. Xie, Y. Park, L. Chen, X. Wang, H. Luan, Y. Yang, H. Wang, C. Liang, Y. Xue, R.D. Schaller, D. Chanda, Y. Huang, Y. Zhang, J.A. Rogers, Proc. Natl. Acad. Sci. U. S. A. 116 (2019) 13239–13248.
[249] M. Park, Y.J. Park, X. Chen, Y.-K. Park, M.-S. Kim, J.-H. Ahn, Adv. Mater. 28 (2016) 2556–2562.
[250] R. Grantab, V.B. Shenoy, R.S. Ruoff, Science 330 (2010) 946–948.
[251] P. Zhang, L. Ma, F. Fan, Z. Zeng, C. Peng, P.E. Loya, Z. Liu, Y. Gong, J. Zhang, X. Zhang, P.M. Ajayan, T. Zhu, J. Lou, Nat. Commun. 5 (2014) 3782.
[252] S.-K. Lee, B.J. Kim, H. Jang, S.C. Yoon, C. Lee, B.H. Hong, J.A. Rogers, J.H. Cho, J.-H. Ahn, Nano Lett. 11 (2011) 4642–4646.
[253] S. Bertolazzi, J. Brivio, A. Kis, ACS Nano 5 (2011) 9703–9709.
[254] Y. Hwangbo, C.-K. Lee, S.-M. Kim, J.-H. Kim, K.-S. Kim, B. Jang, H.-J. Lee, S.-K. Lee, S.-S. Kim, J.-H. Ahn, S.-M. Lee, Sci. Rep. 4 (2014) 4439.
[255] D.-H. Kim, J.-H. Ahn, W.M. Choi, H.-S. Kim, T.-H. Kim, J. Song, Y.Y. Huang, Z. Liu, C. Lu, J.A. Rogers, Science 320 (2008) 507–511.
[256] W.N. Sharpe, J. Pulskamp, D.S. Gianola, C. Eberl, R.G. Polcawich, R.J. Thompson, Exp. Mech. 47 (2007) 649–658.
[257] J.A. Rogers, J.-H. Ahn, Silicon Nanomembranes: Fundamental Science and Applications, Wiley-VCH, Weinhein, Germany, 2016.
[258] A. Taloni, M. Vodret, G. Costantini, S. Zapperi, Nat. Rev. Mater. 3 (2018) 211–224.
[259] Y. Zhu, F. Xu, Q. Qin, W.Y. Fung, W. Lu, Nano Lett. 9 (2009) 3934–3939.
[260] F.W. DelRio, R.F. Cook, B.L. Boyce,Appl. Phys. Rev. 2 (2015), 021303.
[261] G. Brambilla, D.N. Payne, Nano Lett. 9 (2009) 831–835.
[262] W. Liu, Q. Zou, C. Zheng, C. Jin, ACS Nano 13 (2018) 440–448.

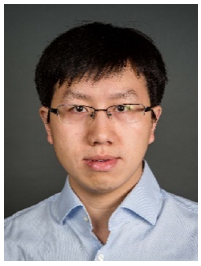

Hangbo Zhao is currently a postdoctoral fellow in the Center for Bio-Integrated Electronics at Northwestern University, USA. He received his B.S. degree (2011) in precision instruments from Tsinghua University, China. He then received his M.S. (2014) and Ph.D. (2017) degrees from the Massachusetts Institute of Technology (MIT), both in mechanical engineering. His research focuses on micro/nano fabrication, 3D assembly, engineered surfaces, and bio-integrated electronics.

Yongjun Lee is pursuing his Ph.D. degree under the supervision of Prof. Jong-Hyun Ahn at the School of Electrical and Electronic Engineering, Yonsei University. His research interests include triboelectric nanogenerators and flexible electronics using two-dimensional materials.

Mengdi Han is a postdoctoral fellow at Center for Bio-Integrated Electronics in Northwestern University, USA. He received his B.S. degree in 2012 from Huazhong University of Science and Technology and his Ph.D. degree in 2017 from Peking University, both in Electrical Engineering. His research interests include bio-integrated electronics, 3D electronic networks, and energy harvesting.

Bhupendra Kumar Sharma obtained his Ph.D. degree from the Indian Institute of Technology Delhi in 2010. Currently, Sharma is working as a Research Professor of the Center for Strain Engineered Electronic Devices at Yonsei University, Korea. His research includes oxides and 2D-material-based electronic devices for stretchable and flexible systems.

Xuexian Chen received her B.S. degree from the University of Electronic Science and Technology of China, Chengdu, in 2015. She is currently pursuing the Ph.D. degree at the National Key Laboratory of Nano/Micro Fabrication Technology, Peking University, Beijing, China. Her current research interests focus on nanogenerators, flexible/stretchable electronics and microrobots.

Prof. Jong-Hyun Ahn is an Underwood distinguished professor in the School of Electrical and Electronic Engineering at Yonsei University, Korea where he also serves as Director of the Center for Strain Engineered Electronic Devices. His research focuses on fundamental and applied aspects of graphene and 2D materials.

Prof. John A. Rogers is the Louis Simpson and Kimberly Querrey Professor in Materials Science and Engineering, Biomedical Engineering, Mechanical Engineering, Electrical Engineering and Computer Science, Chemistry, and Neurological Surgery at the Northwestern University where he also serves as Director of the Center for Bio-Integrated Electronics. His research focuses on unusual electronic and photonic devices, with an emphasis on biointegrated and bioinspired systems. He is a member of the National Academy of Sciences, the National Academy of Engineering, the National Academy of Medicine, and the American Academy of Arts and Sciences.